

Review

Recent status and challenging perspective of high entropy oxides for chemical catalysis

Yi Wang,^{1,3,4} Jinxing Mi,^{1,4} and Zhong-Shuai Wu^{1,2,*}

SUMMARY

High entropy oxides (HEOs) have attracted wide interest for chemical catalysis owing to abundant active sites, adjustable specific surface area, stable crystal structure, extraordinary geometric compatibility, and unique electronic balance factors, exhibiting huge potential value for commercial exploitation. Here, the recent progress and current challenges of HEOs from the typical synthetic strategies, unique structural features, and intrinsic properties to applications in both thermocatalysis and electrocatalysis are comprehensively summarized. In brief, the HEOs obtained by different synthetic strategies, along with their structural features and derived physical-chemical properties endowed by the entropy-driven effect, allow them with highly efficient catalytic application performance. More important, the remarkable enhancement of catalytic performance based on the pure and modified HEOs are discussed by analyzing reaction mechanisms to further motivate the development in this emerging field. Finally, the future directions and challenging perspectives for chemical catalysis over HEOs are also put forward.

INTRODUCTION

The establishment and application of materials science is important to drive social development and progress effectively. Composed by one or more kinds of chemical elements, the designed materials own specific structures along with abundant physical-chemical properties, which play a key role in guaranteeing the development of energy catalysis and controlling environmental pollution for all of human society.^{1,2} Therefore, the exploration and utilization of new materials, including but not limited to metallic materials, inorganic non-metallic materials, and polymer materials, have never been interrupted. Especially for metallic materials, its application not only covers a wide range of people's basic necessities of life, but also involves the various kinds of industrial fields of social development.^{3,4} Among the metallic materials, high-entropy materials (HEMs) have attracted wide attention due to their unique features, such as the stable solid solutions with well-defined crystal structures and abundant constituent elements.^{5–7} By virtue of the structural characteristics, including lattice distortion, slow diffusion effect, and high entropy effect, HEMs possess excellent instinct properties such as high-temperature resistance, strong mechanical stability,⁸ corrosion resistance, and high work hardening, which are superior to those of most traditional metallic materials.⁹ Moreover, as a class of materials, HEMs not only contain oxides,¹⁰ but also include alloys,¹¹ carbides,¹² fluorides,¹³ and sulfides¹⁴ (Figure 1). More important, the recent key progress of HEMs represents a major breakthrough in the development of materials science and provides a feasible reference for the research and development of other types of materials by using multi-principal elements to improve their specific properties and application

The bigger picture

The development of materials science and catalysis technology plays a significant role in promoting human and social progress. The catalytic utilization of high entropy materials (HEMs) has attracted intense attention for chemical catalysis because of their superior thermostability and variable chemical properties. In particular, the high entropy oxides (HEOs) demonstrate huge potential for thermocatalytic and electrocatalytic applications. Modifying HEOs catalysts for targeted reactions would be a promising technical step toward the development of materials science and catalysis technology. Moreover, HEOs also have been confirmed to be active for many thermocatalysis (heterogeneous and homogeneous) fields, electrocatalysis fields, and energy storage applications. This review summarizes the recent developments and challenging perspectives of HEOs for chemical catalysis, which are of great importance to guide the future directions of emerging HEO-based catalysis.

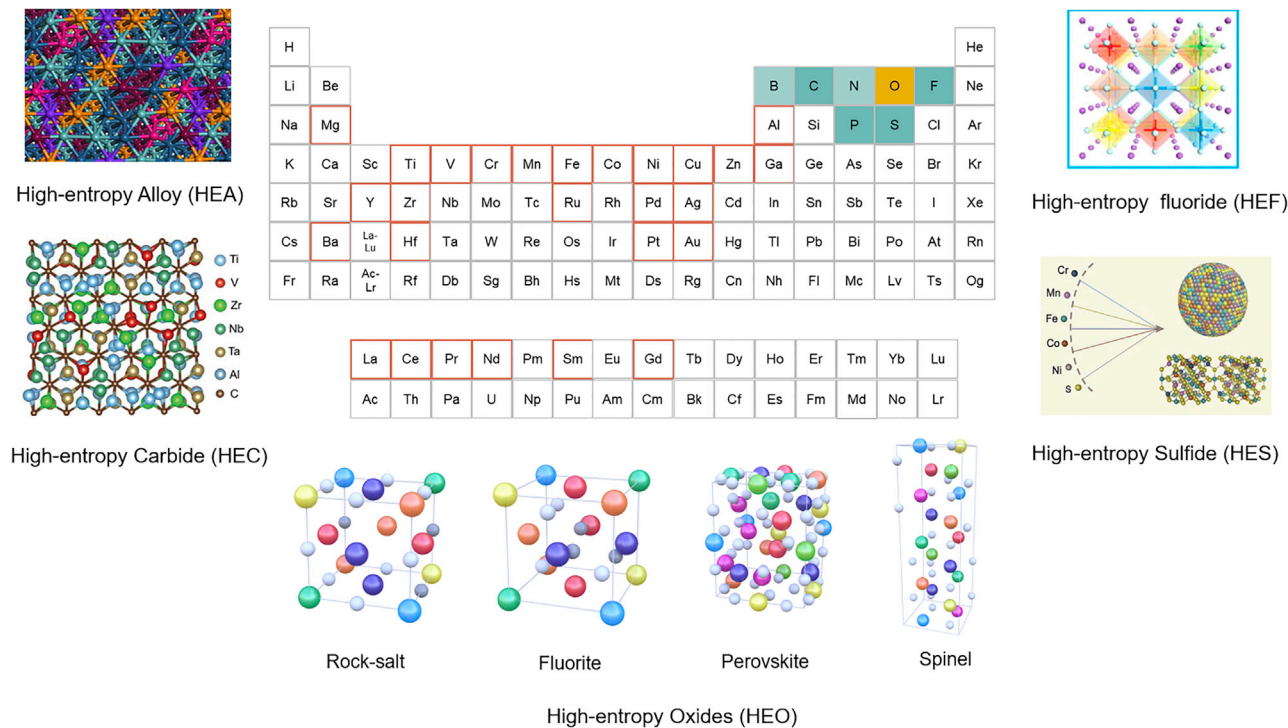


Figure 1. Categories of HEMs and phase structure of HEOs

potential. Among these HEMs, the high entropy oxides (HEOs) have been focused on its environment-friendly synthesis methods and abundant catalytic applications due to the demand of metal oxides and easily modified properties (e.g., redox ability, stable chemical state).^{10,15,16} Moreover, HEOs are also easier than other HEMs to combine with active noble metal species for different catalytic applications. According to crystal structures, HEOs could be divided into four styles of rock salt-type HEOs (R-HEOs), fluorite-type HEOs (F-HEOs), perovskite-type HEOs (PE-HEOs), and spinel-type HEOs (SP-HEOs) (Figure 1).^{17–20} At first, only single-phase HEOs could be thought of as HEOs. With their rapid development, the HEOs in the mixed phase could also be regarded as HEOs, which further extends their application fields and enriches functionalities. That is because the HEOs in the mixed phase own more interfaces and junctions, which can still keep the stable structure and adjustable physical-chemical properties. With the above excellent features, HEMs (mainly for HEOs) have been widely used in various applications, such as electrode,²¹ ceramic material,⁶ semiconductor,²² energy storage,⁹ and catalysis.⁷

As mentioned above, HEOs are one kind of oxide system composed mainly of multiple equi-atomic metal elements.¹⁰ Combined with the ideal configurational entropy ($\Delta S_{\text{conf}} = -R \sum_{i=1}^n x_i \ln x_i$) concept and the Gibbs-Helmholtz equation ($\Delta G_{\text{mix}} = \Delta H_{\text{mix}} - T \Delta S_{\text{mix}}$), it is found that the HEOs ($\Delta S_{\text{mix}} \geq 1.5R$) could be well generated only when the number of equimolar cations to construct the mixed metal oxides is greater than or equal to 5 (Figure 2A).²³ Moreover, the equimolar cations in the structure of HEOs are distributed randomly (Figure 2B), thus exhibiting unexpected functionalized behaviors.²⁴ Meanwhile, the corresponding elemental distribution maps (Figure 2C) and extended X-ray absorption fine-structure (EXAFS) spectroscopy results (Figure 2D) also confirmed the homogeneity of HEOs, with metal elements distributed disorderly in the phase structure.¹⁶ Through

¹State Key Laboratory of Catalysis, Dalian Institute of Chemical Physics, Chinese Academy of Sciences, 457 Zhongshan Road, Dalian 116023, China

²Dalian National Laboratory for Clean Energy, Chinese Academy of Sciences, 457 Zhongshan Road, Dalian 116023, China

³University of Chinese Academy of Sciences, 19 A Yuquan Road, Shijingshan District, Beijing 100049, China

⁴These authors contributed equally

*Correspondence: wuzs@dicp.ac.cn

<https://doi.org/10.1016/j.cheecat.2022.05.003>

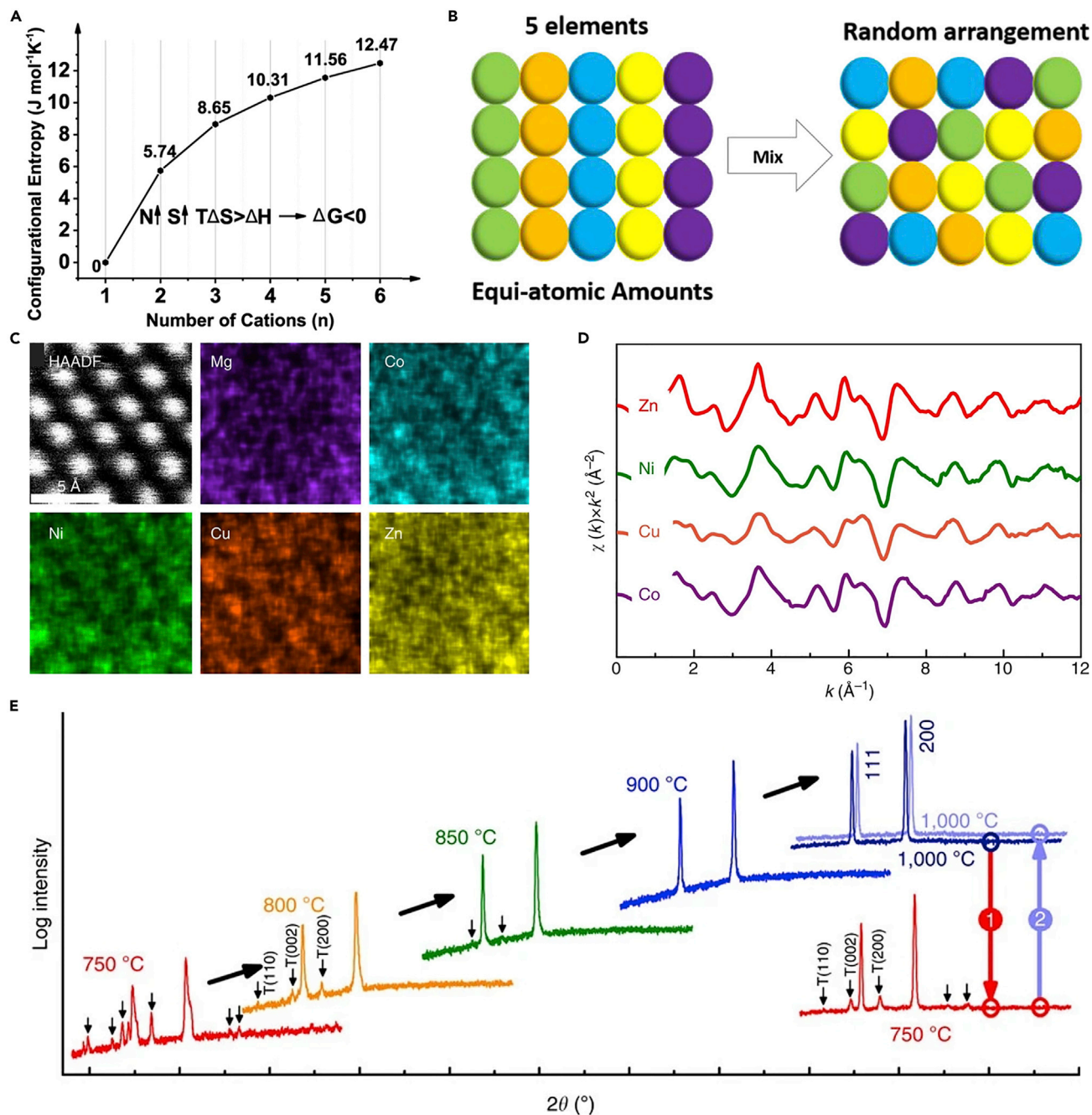


Figure 2. Structure features of HEOs

(A) Configurational entropy of HEOs. Adapted with permission from Zhang et al.²⁸

(B) Equi-atomic, semi-radii components before and after mixing. Adapted with permission from Albedwawi et al.²⁴

(C) High-angle annular dark field (HAADF) image of ZnNiCuMgCo HEOs. Adapted with permission from Rost et al.¹⁶

(D) EXAFS measured at advanced photon source beamline 12-BM after energy normalization and fitting. Adapted with permission from Rost et al.¹⁶

(E) XRD patterns of ZnNiCuMgCo HEOs at different conditions. Adapted with permission from Rost et al.¹⁶

the macro-point, there is only one crystalline phase for the HEOs. As shown in Figure 2E, the rock salt structure could only be formed after treatment above 900°C for R-HEO, while the multiple rock salt structures emerged at 750°C. Notably, the single-phase state appeared again when once more treated at 1,000°C; that is,

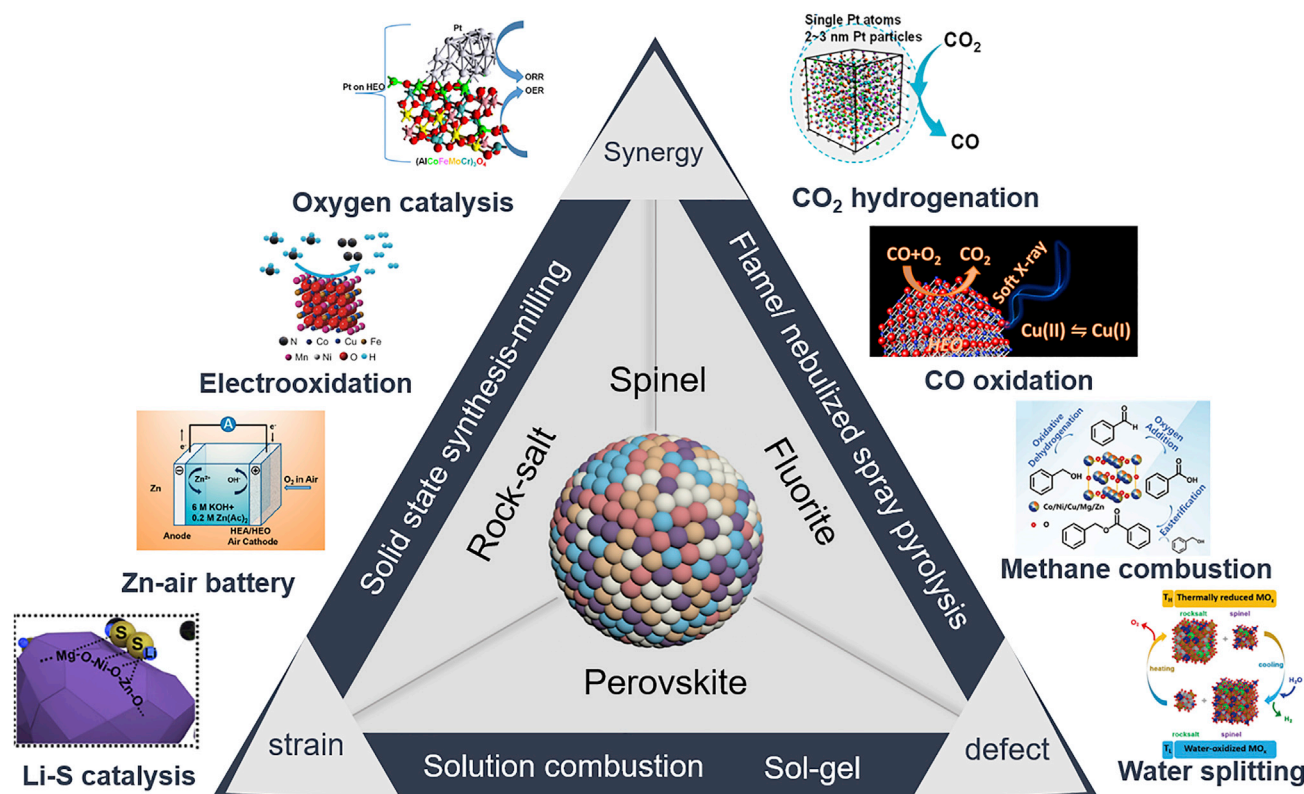


Figure 3. Synthesis, properties, and catalytic applications of HEOs

because the low temperature could not guarantee the enthalpy-driven phase separation. In particular, this enthalpy-driven phase separation phenomenon contributes to its excellent structure stability at high temperature, similar to complicated compound systems.^{16,25} The successful application of HEOs into various kinds of fields has already expanded their directions and stimulated interesting inspirations. Among the applications of HEOs above, chemical catalysis reactions bring about much attention. Therefore, HEOs are considered a perfect platform for the building of thermocatalytic development. Not only the preparation methods but also various kinds of activation strategies have been studied to enhance their catalytic performance.^{8,26,27} Based on these principles, HEOs, as pure catalyst or support to integrate with active sites, have also been developed for various catalytic applications. Despite the effective development of HEOs for catalytic applications, a comprehensive and instructive topic review is urgently needed to highlight the recent status and challenging perspective of HEOs.

In this review, the recent advances of key synthesis strategies and unique properties of HEOs for chemically catalytic applications of thermo- and electrocatalysis are summarized thoroughly (Figure 3).^{15,29–35} We not only describe the preparation of HEOs and their catalytic applications but we also overview the key synthesis strategies to endow active sites (e.g., noble metal) into the framework of HEOs to attain various kinds of catalysts with enhanced performance. First, we mainly focus on the synthesis strategies of HEOs by traditional (e.g., the ball-milling method) and novel methods (e.g., sol-gel and plasma spraying methods) to compare their advantages and disadvantages. Second, we further introduce the applications of HEOs in the catalysis fields of thermocatalysis (e.g., CO oxidation, CO₂ hydrogenation) and

electrocatalysis (e.g., oxygen catalysis, Li-S battery catalysis) and elucidate their reaction mechanisms. Meanwhile, some other key reactions (e.g., water splitting, methane combustion) catalyzed by HEOs are also illustrated. Finally, we discuss the emerging challenging issues of HEOs for chemical catalysis and propose key future development directions. We believe that these observations here could greatly motivate the continuous pursuit of HEOs in both adjustable preparation and diversified catalytic applications.

SYNTHESIS OF HEOs

As one novel class of promising HEMs, HEOs with stable geometric structures and unique electronic properties have attracted extensive research in the catalysis field. Moreover, the synthesized HEOs with abundant active sites, high specific surface area, and stable multi-component single phase is the key to original catalytic performance. For the generated HEOs, the participated cations not only dominate the behaviors and properties of materials but also affect the geometric compatibility and electronic balance factors.^{16,18,24,36} In this section, we highlight typical well-established synthetic methods for preparing HEOs, and provide an efficient discussion and outlook on their generality and effectiveness.

Solid-state synthesis

Solid-state synthesis is a traditional method for preparing HEOs. In detail, the metal oxides in equimolar proportions are mixed, mechanically ground, pressed, and quenched in an oxygen atmosphere to obtain a fixed-structure high-entropy solid solution.^{37–39} Fabulous long-term mixing is the key step for the generation of homogenization and single-phase materials, while the quenching process realizes its structural stability at high temperatures. The kind and content of cations determine the properties and functionalized behaviors of the generated HEOs.⁴⁰ Specifically, the value of the cation radius of each component is similar and the crystal structure of at least one cation is different, forming a single-phase oxide with a unique electronic structure.³⁸ In 2015, single-phase rock salt-type HEOs were first proved by Rost and co-workers through this synthesis strategy.¹⁶ Since then, stable oxides with high configuration entropy have emerged endlessly, with excellent dielectric properties, intrinsic mechanical properties, thermal stability, and magnetic properties. For instance, Dragoie et al.⁴¹ synthesized (Mg, Cu, Ni, Co, Zn) O material substituted with monovalent cations (Li^+ , Na^+), which exhibited an inherent charge compensation mechanism involving oxygen vacancies. Therefore, the ionic conductivity of Li^+ exceeds $10^{-3} \text{ S cm}^{-1}$ at room temperature, providing an effective way for the rapid diffusion of Li^+ or Na^+ and promising applications as solid-state electrolytes. Moreover, the solid-state synthesis methods have been widely applied to obtain various HEOs for their functionalized applications.^{29,42} For catalysis, precisely regulating the diverse nanostructured morphology of HEOs (e.g., nanowires, nanosheets, nanospheres, nanoplates, nanorods) can efficiently expose specific catalytic crystal planes and active sites to improve the catalytic performance.

Flame spray (FSP) and nebulized spray pyrolysis (NSP)

FSP and nebulized spray pyrolysis NSP are the simplified scalable synthesis technologies used to prepare HEOs.^{18,43} The FSP technology atomizes the precursor solution containing the appropriate combination of atoms and cations into a fine aerosol mist by an ultrasonic atomization device, which is injected into a self-sustaining flame through flowing oxygen and pyrolyzing to form a uniform oxide.⁴⁴ The generated aerosol stays in the flame for a short time to inhibit the growth of oxidized particles, and the oxidized particles are quickly heated in the flame chamber maintained at a subambient pressure (60 mm) and then quenched to room temperature. Finally,

ultra-fine powder was obtained. Similarly, for the NSP method, the precursor solution is atomized under similar conditions and transported into the tube furnace, with oxygen as the carrier gas, calcinated at high temperature.⁴⁵ As relatively fast processes, both FSP and NSP not only significantly shorten the synthesis time but also stabilize the metastable phase due to their rapid quenching effect, exhibiting a higher industrial application potential because of their high-efficiency yield characteristics.^{46,47} For instance, Sarkar et al.⁴⁸ synthesized rock salt structure ($\text{Co}_{0.2}\text{Cu}_{0.2}\text{Mg}_{0.2}\text{Ni}_{0.2}\text{Zn}_{0.2}$) O HEOs through the NSP method as an anode for energy storage. It is found that the entropy stabilization effect of the crystal lattice maintains the primary and permanent structure in the conversion cycle, consequently contributing to the high-capacity retention and excellent delithiation behavior. Moreover, the controllable porous hollow structure and specific surface area could facilitate the tuning of catalytic performance based on rapid solvent evaporation and solute decomposition.

Solution combustion synthesis (SCS)

SCS is a combustion-based method to prepare materials with high crystallinity relying on the rapid self-sustained exothermic reaction, which has the advantages of high efficiency (controlled reaction condition) and high product purity.^{49,50} During the process, the composition and content (fuel:oxidizer ratio [ϕ]) along with the reaction system are the key factors to affect the performance of as-synthesized powder.⁵¹ Specifically, the precursors metal nitrate (e.g., carbonate, sulfate) as oxidant and glycine (e.g., citric acid, amino acid) as complexing agent and fuel were mixed into a uniform solution for heating spontaneous combustion after solution evaporation, realizing the low-temperature synthesis.⁵² In 2018, Khaki's group⁵³ studied the influence of the above reaction condition on the performance of synthetic powder, laying the foundation for future methodology. Furthermore, SCS is an effective method to synthesize HEOs with unique physical and chemical properties at low temperatures. Salimi et al.⁵¹ determined the fuel type and fuel consumption in combination with thermodynamic calculations and calculated the effect of activity coefficient changes on single-phase HEOs. Based on this theory, they used different fuels and controlled the reaction conditions to synthesize single-phase HEOs with extraordinary physiochemical properties (Figure 4), thereby summarizing the optimal synthesis path. As a result, it is revealed that the single-phase HEO powder synthesized under fuel-lean conditions with glycine as raw material displays outstanding crystallinity, particle size, high porosity, specific surface area, and thermal stability. This provide a good reference for the precise regulation of HEOs for catalytic application.

Sol-gel method

The sol-gel method refers to the inorganic or metal alkoxides forming a complete three-dimensional (3D) network structure through a solution sol-gel process along with post-treatment,²⁵ which involves the hydrolysis and condensation, depending on their unique characteristics.⁵⁴ Compared with the solid-phase synthesis, the sol-gel method has inherent advantages for synthesizing uniform and dense HEO powder, which is reflected in the following aspects: (1) the mild low-temperature preparation avoids excessive sintering and deactivation of the material for the catalytic process;⁵⁵ (2) controllable preparation of multiple crystal structure materials (e.g., spinel, fluorite, perovskite); and (3) the obtained material presents good texture parameters, unique morphology, optimized pore size distribution, and phase stability.⁵⁶ For example, Kim's group⁵⁴ synthesized high-entropy rare earth oxides (HE-RE-Os) with Y, La, Ce, Nd, and Gd by the milling method and the sol-gel method (Figure 5). The as-grown HE-RE-Os by the sol-gel method demonstrated composition uniformity, high specific surface area, and abundant porosity, with a

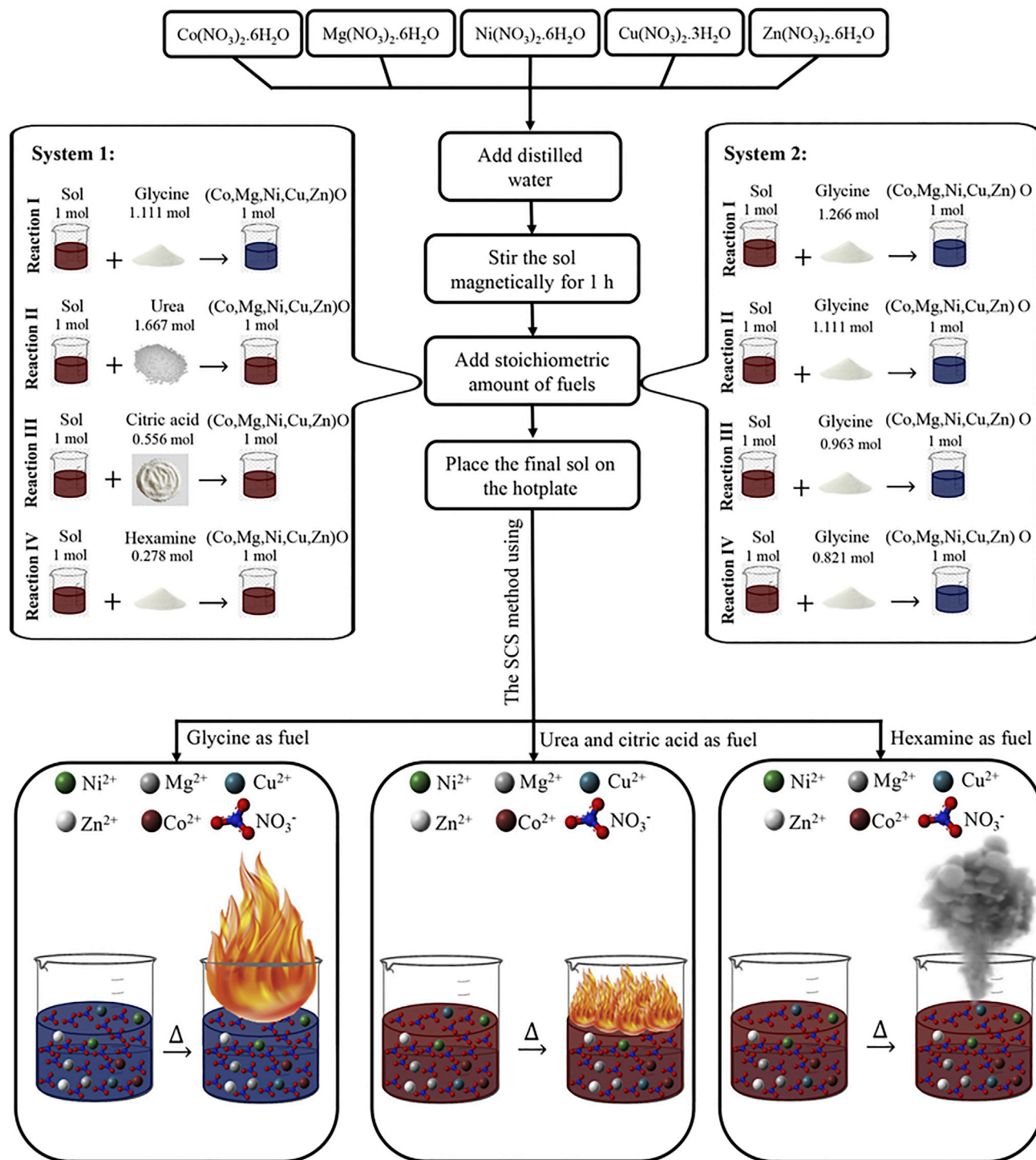


Figure 4. Schematic diagram of SCS procedure of HEOs

Adapted with permission from Salimi et al.⁵¹

lower annealing temperature, applying to synthesize high-quality ceramic materials. Furthermore, the formation mechanism, microstructure, stability, and performance of the material, together with the superiority of the synthesis strategy, are highlighted, laying the foundation for the efficient synthesis of other HEO materials. In

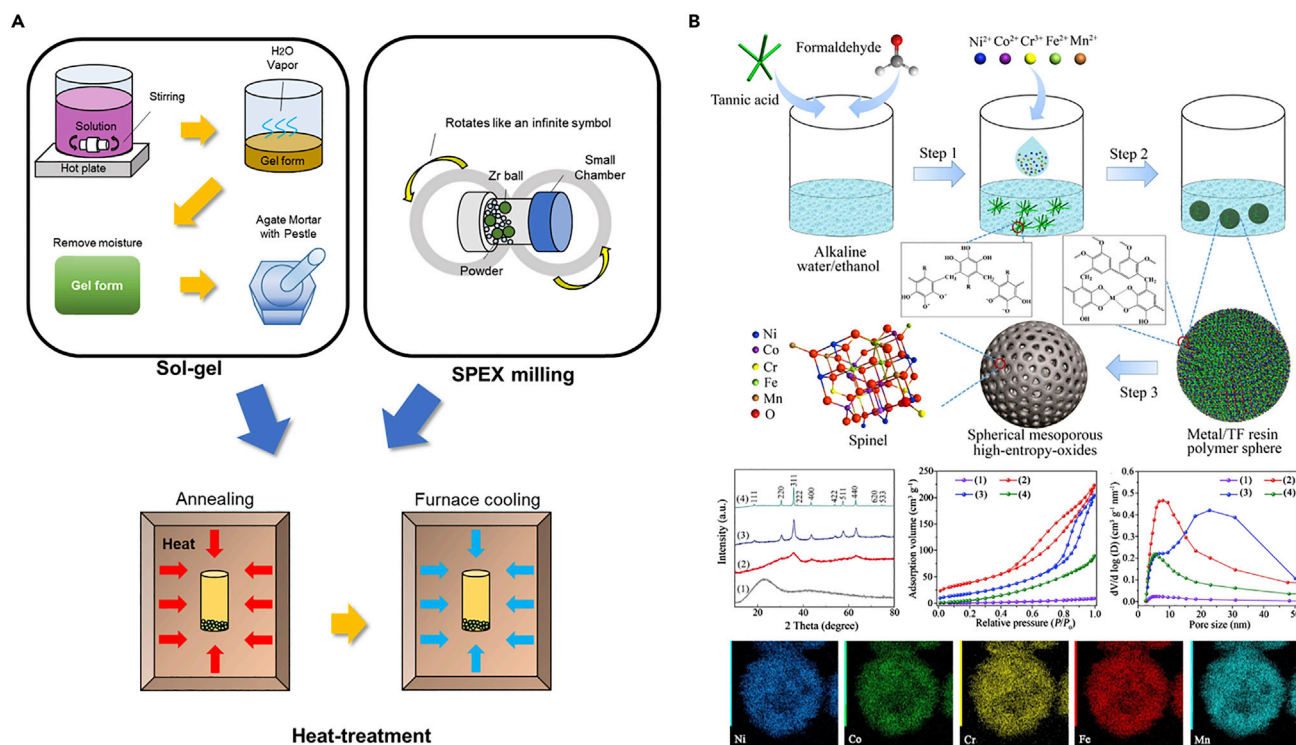


Figure 5. Sol-gel method for fabricating HEOs

(A) Schematic of sol-gel and milling method of HE-REO. Adapted with permission from Kim et al.⁵⁴

(B) Schematic of the synthetic procedure of HEOs, and their characterizations. Adapted with permission from Wei et al.²⁵

In addition, using polyphenols as a polymerizable ligand, Wei's group²⁵ synthesized high-entropy spinel oxides having unique spherical morphology, a large surface area, and mesoporous characteristics by the sol-gel method (Figure 5B). It is found that controlling the hydrolysis-condensation rate of the five metal sources and maintaining the morphological characteristics and mesoporous structure stability at the crystallization process under high-temperature are the key steps to the synthesis of hollow mesoporous HEOs. The composited metal elements are evenly distributed, benefiting from the catechol groups and metal-chelating ability of polyphenols, and then thermally decomposing to obtain a hollow spherical structure, which exhibits robust performance of degradable organic pollutants. Moreover, this synthetic strategy can also be extended to other high-entropy nanomaterials to construct their unique structure.⁵⁴

Besides the typical synthesis methods above, sonochemical,⁵⁷ hydrothermal,⁵⁸ microwave-assisted precipitation,⁵⁹ atmospheric plasma spraying,⁶⁰ flash sintering,⁶¹ and electrospinning⁶² techniques were reported to synthesize HEOs with specific morphology and structure, exhibiting excellent mechanical strength, dielectric properties, magnetism, and thermal stability. It is believed that the continuous innovation and development of synthesis strategies promote the emergence of other HEMs (e.g., carbides, borides, sulfides), providing a new direction for applications in the catalytic and energy conversion fields.

HEOs FOR CATALYTIC APPLICATIONS

Based on the above discussion, HEOs could be prepared by various methods to exhibit superior physiochemical properties for various functional applications.¹⁰

Here, we in detail discuss, analyze, and concisely summarize the recent developments in HEOs for classical and important thermocatalysis (CO oxidation, CO₂ hydrogenation) and electrocatalysis (oxygen evolution reaction, oxygen reduction reaction, electrooxidation, and Li-S batteries) applications. It is noted that not only abundant experimental techniques but also primary theoretical works have been used to explore the structure-function relationship between HEO catalysts and their physical-chemical properties.

CO oxidation

As one classical thermocatalysis reaction, CO oxidation has been commercially applied and explored in depth because of its significant promoted effect on air purification from toxic gases.⁶³ To date, transition metals oxides such as Cu, Fe, Co, and Mn-based oxides are confirmed to be active for CO oxidation. The excellent catalytic performance of transition metal oxides for CO oxidation is promoted by their abundant surface-activated oxygen (mainly lattice oxygen), which impairs the rate-limiting step for CO oxidation and keeps its functionalities under cycling conditions.^{64,65} Meanwhile, noble metals (e.g., Au, Pt, and Pd) are usually doped into the above transition metal oxides to optimize their low-temperature catalytic activity.^{66,67} As one kind of compound combining and concentrating multifarious transition metals oxides, HEOs exhibit great potential for CO oxidation under varied conditions and own the ability to incorporate with noble metals, as discussed below.

By virtue of the novel desirable properties of HEOs, D'Angelo et al.⁶⁸ reported classical HEOs Mg_{0.2}Co_{0.2}Ni_{0.2}Cu_{0.2}Zn_{0.2}O for CO oxidation by advanced *in situ* spectroscopy techniques, along with theoretical simulation. As shown in Figure 6A, the as-obtained Mg_{0.2}Co_{0.2}Ni_{0.2}Cu_{0.2}Zn_{0.2}O was constituted by a central Cu²⁺ site along with six O in an octahedron in the rock salt phase. As a result, Cu²⁺ cations, which coordinated over the immediate surface, are identified as contributing to the Cu L_{2,3}-edge spectrum in these HEOs. When applied for CO oxidation, the increased reduced Cu⁺ sites could activate CO to generate bidentate carbonate, which is beneficial to subsequent oxidation reactions. Moreover, a theoretical basis of the HEOs for CO oxidation through the molecular collision between O₂ and adsorbed CO from Cu⁺ sites over HEOs was also proved by Fourier transform infrared spectroscopy. Meanwhile, Fracchia et al.³⁰ studied the role of other elements in these HEOs for CO oxidation (Figure 6B). Unexpectedly, only the Cu species are active, while Co and Ni species do not work at all in the CO oxidation reaction. Specifically, the reduction transforms of Cu²⁺ to Cu⁺ by CO above 130°C, as well as the oxidation transform of Cu⁺ to Cu²⁺ under the O₂ atmosphere above 250°C, allow excellent CO catalytic oxidation performance of HEOs. It should be noted that this cyclic transform between Cu²⁺ to Cu⁺ could not easily occur over pure CuO above 100°C because of its stability. In short, it is theoretically proved that the unique high entropy effect of HEOs could stabilize their structure and keep the reversibility of oxidation/reduction of Cu species, which is beneficial to the catalytic cycle of CO oxidation.

Traditional HEOs usually have a limited specific surface area with a poor porous structure, which is not good for the gas-solid heterogeneous catalysis reaction. To solve this issue, Zhang et al.⁶⁹ used the solid sol-gel strategy to obtain Cu-based HEOs with abundant mesoporosity (Figure 6C). In this process, organic and inorganic metal salts, along with surfactants, were mechanically ground after the efficient assembly. After washing and drying, the mesoporous metal oxides were obtained through further calcination. As desired, the as-obtained (CuNiFeCoMg) O_x-Al₂O₃ catalyst exhibited a high specific surface area (198 m² g⁻¹) in the form of

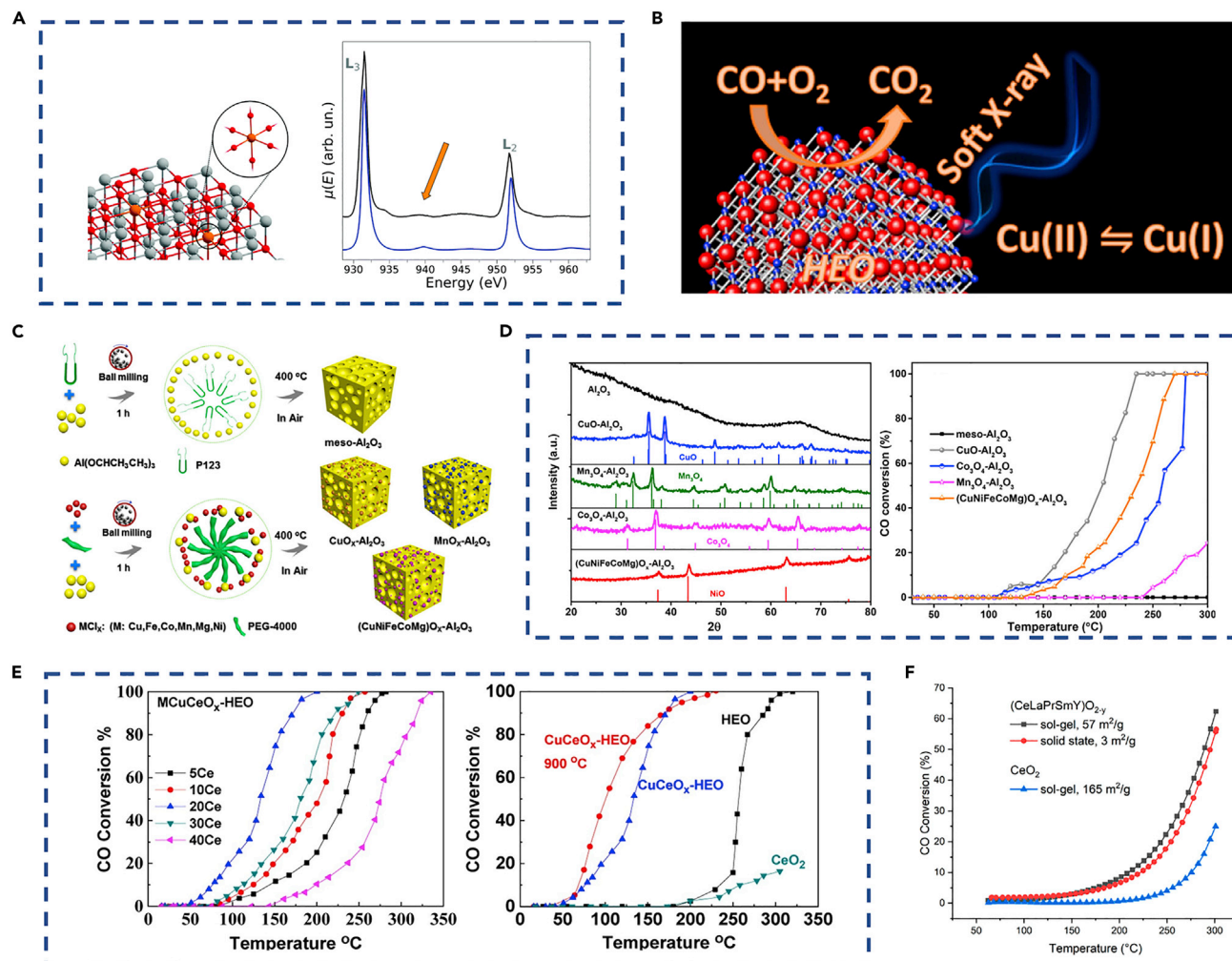


Figure 6. Preparation and structure of HEOs and thermocatalytic application in CO oxidation

(A) Left: Three-dimensional rendering of the HEOs surface. Right: Experimental (black line) and theoretical (blue line) Cu $L_{2,3}$ -edge spectra of the pristine HEOs. Adapted with permission from D'Angelo et al.⁶⁸

(B) Schematic diagram of $\text{Cu}^{2+} \rightarrow \text{Cu}^+$. Adapted with permission from D'Angelo et al.³⁰

(C) Synthesis schematic of meso- Al_2O_3 . Adapted with permission from Zhang et al.⁶⁹

(D) Left: XRD patterns. Right: CO oxidation activity of different catalysts. Adapted with permission from Zhang et al.⁶⁹

(E) Left: CO conversion over $\text{MCuCeO}_x\text{-HEO}$ catalysts. Right: CO conversion over $\text{CuCeO}_x\text{-HEO}$ and $\text{CuCeO}_x\text{-HEO}$. Adapted with permission from Chen et al.⁷⁰

(F) CO oxidation activity of $(\text{CeLaPrSm})\text{O}_{2-y}$ and comparison catalysts. Adapted with permission from Riley et al.⁵⁶

pure phase, and showed impressive enhanced CO oxidation performance. Due to the structure stability, $\text{CuO-Al}_2\text{O}_3$ and $(\text{CuNiFeCoMg})\text{O}_x\text{-Al}_2\text{O}_3$ also exhibited outstanding catalytic CO conversion in a span of 48 h. In agreement with the density functional theory (DFT) results, it is confirmed that the HEOs have a superior and stable conversion ability of CO oxidation. Moreover, Cu-based HEOs also can protect themselves from SO_2 poisoning, indicating a potential adaptation ability in complicated industrial conditions.

Although the stable CO conversion ability with good SO_2 resistance could be achieved over Cu-based HEOs, the poor low-temperature performance limits further development. To this end, Chen et al.⁷⁰ reported a novel method to prepare an HEO-based catalyst with remarkable catalytic performance in the whole

reaction range for CO oxidation through combining HEOs and CuCeO_x . CuCoNiMgZn HEOs were obtained through the ball-milling method along with calcination, using the chlorate and CeO_2 obtained from the calcination of $\text{Ce}(\text{NO}_3)_2 \cdot 6\text{H}_2\text{O}$. As a result, the CO could be oxidated over these MCuCeO_x -HEO catalysts even below 50°C ; the origin conversion temperature is much lower than that of $(\text{CuNiFeCoMg})\text{O}_x\text{-Al}_2\text{O}_3$ (Figure 6E). The CO conversion rates of these MCuCeO_x -HEOs catalysts increased and were kept stable with increasing reaction temperature. The 20% CuCeO_x -HEO catalyst displayed the highest CO conversion (CO reacted at $\sim 50^\circ\text{C}$ and fully reacted at $\sim 200^\circ\text{C}$) among these MCuCeO_x -HEOs. Moreover, CuCeO_x -HEO catalyst not only exhibited much higher catalytic activity (especially for low-temperature activity) than pure HEOs and CeO_2 catalyst but also maintained superior performance even after thermal treatment under 900°C for 4 h (Figure 6E). It is disclosed that the regulation of the physiochemical properties of HEOs could further enhance low-temperature performance and SO_2 resistance. Unexpectedly, not only transition metal HEOs but also rare earth element HEOs also had a better CO conversion ability than those of pure rare earth oxides. For example, Riley et al.⁵⁶ designed a facile sol-gel method to obtain rare earth-type HEO ($\text{CeLaPrSmY})\text{O}_{2-y}$. Although the as-obtained $(\text{CeLaPrSmY})\text{O}_{2-y}$ through the sol-gel method has a higher surface area ($57 \text{ m}^2 \text{ g}^{-1}$) than that obtained by the solid-state method ($3 \text{ m}^2 \text{ g}^{-1}$), both demonstrate similar CO conversion in the whole reaction temperature, while they are much better than that of pure CeO_2 (Figure 6F). To summarize, the introduced metal species could possess active chemical states (such as the transform between Cu^{2+} and Cu^+) in the form of HEOs, thereby exhibiting enhanced CO oxidation performance. Meanwhile, the active chemical state, along with stable crystal structure, contributes to superior catalytic stability under complicated conditions.

Regulating HEOs could improve the catalytic CO oxidation ability to a certain extent under harsh conditions. Therefore, other strategies, such as the combination of noble metals and HEOs, were taken to maximally optimize CO oxidation performance. For instance, Chen et al.⁷¹ reported a strategy to obtain Pt-based HEO catalysts with excellent catalytic activity and intrinsic high-temperature stability. Specifically, the NiMgCuZnCoO_x was prepared by ball-milling and subsequent calcination at 900°C (Figure 7A). As for PtNiMgCuZnCoO_x HEOs, metal salt (equal molar) is dissolved in water with cetyltrimethyl ammonium bromide. After stirring, a certain amount of H_2PtCl_6 in H_2O was added and then stirred constantly with ammonium hydroxide to mix them well. At last, the pure phase PtNiMgCuZnCoO_x HEOs could be achieved through drying and calcination at 900°C . From Figure 7B, it is observed that the introduction of Pt species (only 0.3 wt % Pt) into the NiMgCuZnCoO_x could obviously enhance catalytic CO oxidation performance in the whole temperature range, especially at low temperatures, which is promoted by the generated Pt and PtO_x (Pt-O-M) in the HEOs structure. Moreover, the active Pt-O-M species over 0.3 wt % PtNiMgCuZnCoO_x HEO is also very stable, even after calcination at 900°C . Therefore, the resultant HEOs exhibit superior thermostability at 135°C in a run of 40 h without activity sacrifice. We conclude that the combination of Pt and these transition metals in the form of HEOs could guarantee both high catalytic activity and outstanding high-temperature stability in CO oxidation, surviving under industrial conditions. Except for Pt, other noble metals (including but not limited to Ru, Au, and Pd) could also be incorporated into HEO structures to enhance their CO oxidation ability. Different from the combination of Pt and HEOs at high temperatures,⁷¹ a low-temperature strategy was developed by Okejiri et al.⁵⁷ to obtain HEPO nanoparticle catalysts by the ultrasonication-based method. During the synthesis process, they added

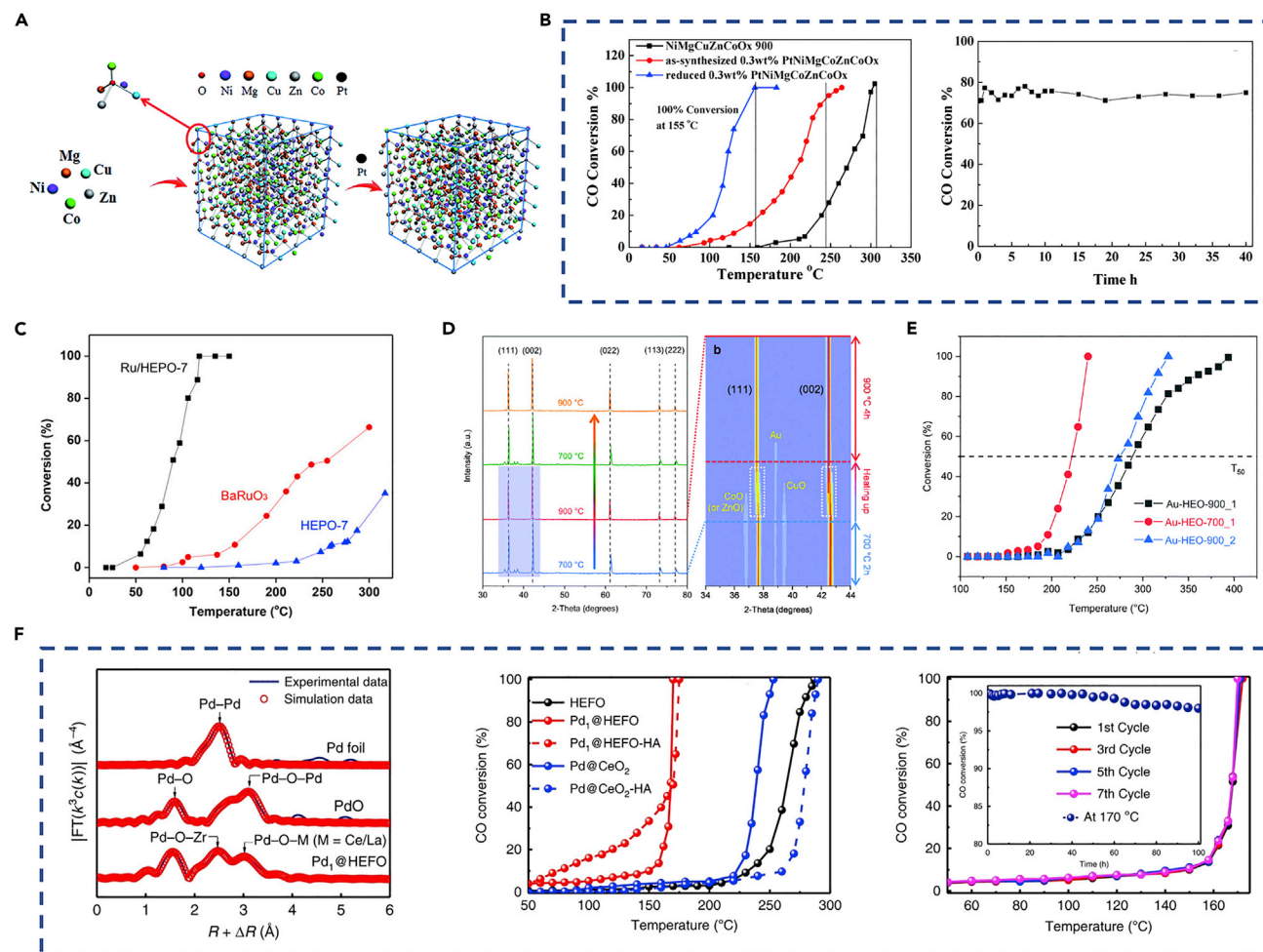


Figure 7. Structure characterization and CO oxidation of HEOs

(A) Synthetic scheme of 0.3 wt % PtNiMgCuZnCoOx. Adapted with permission from Chen et al.⁷¹
 (B) Left: CO oxidation activity of 0.3 wt % PtNiMgCuZnCoOx. Right: Stability of reduced 0.3 wt % PtNiMgCuZnCoOx at a temperature of 135°C for CO oxidation. Adapted with permission from Chen et al.⁷¹
 (C) Light-off curves of CO conversion over different catalysts. Adapted with permission from Okejiri et al.⁵⁷
 (D) Left: Temperature-dependent XRD patterns. Right: *In situ* XRD intensity map. Adapted with permission from Chen et al.⁴²
 (E) CO oxidation of Au-HEO-900 and Au-HEO-700. Adapted with permission from Chen et al.⁴²
 (F) Left: The k^3 -weighted Fourier transforms of Pd K-edge EXAFS spectra. Center: CO conversion of catalysts before (solid lines) and after (dashed lines) hydrothermal treatments. Right: The cycled measurement and stability (170 °C) of CO oxidation over Pd1@HEFO catalyst. Adapted with permission from Xu et al.²⁷

the metal chlorate into the sonication glassware with a NaOH solution. Afterward, the reactants were treated by ultrasonic irradiation to sonicate under ambient conditions. Then, the resultant precipitate was washed and dried at 80°C to obtain the Ba_{0.4}Sr_{0.4}Bi_{0.2}(Zr_{0.3}Hf_{0.3}Ti_{0.2}Fe_{0.2})O₃ (HEPO-7) and Ru_{0.13}/Ba_{0.3}Sr_{0.3}Bi_{0.4}(Zr_{0.2}Hf_{0.2}Ti_{0.2}Fe_{0.27})O₃ (Ru/HEPO-7). Notably, the obtained HEPO-7 and Ru/HEPO-7 have considerable Brunauer-Emmett-Teller (BET) surface areas of 53.9 and 85.5 m² g⁻¹, respectively. From Figure 7C, 51% CO conversion was reached at 90°C along with complete conversion at 118°C for the Ru/HEPO-7 catalyst. Meanwhile, the HEPOs catalyst is almost inactive for CO oxidation conversion below 250°C. To summarize, the excellent catalytic performance of Ru/HEPO-7 catalyst for CO oxidation was mainly enhanced by the well-distributed Ru species in the HEPOs' structure and the synergistic effect between Ru species and HEPOs' structure.

As discussed above, it can be concluded that the incorporation of noble metal into HEOs could maintain excellent thermostability with enhanced low-temperature activity for CO oxidation. To explore the interaction between noble metals and HEOs, Chen et al.⁴² prepared the Au-based HEOs by introducing Au into HEOs at 900°C. Then, a reversible temperature (switch between 700°C and 900°C) is designed for Au-HEOs by temperature-dependent X-ray diffraction (XRD) patterns. As shown in Figure 7D, the appearance and disappearance of the weak peaks of these metal oxides and Au were observed with a diffraction peak shift, which was caused by the lattice compression and expansion of HEOs when circulating temperatures. Clearly, the XRD patterns (Figure 7D) indicated the lattice expansion of HEOs due to Au incorporation along with the disappearance of peaks of CuO and CoO (or ZnO) when the temperature increased. However, the peak of Au(111) could sustain longer even at 900°C. Au could be switched through dissolution and exsolution in the HEOs lattice at 900°C and 700°C, respectively. As a result, the Au-HEO-900 catalyst exhibited a worse catalytic performance than that of Au-HEO-700 for CO oxidation (Figure 7E), due to the decomposing of Au species over Au-HEO-900. Accordingly, the stable state of noble metal species over HEOs, driven by the dissolution of noble metals into the structure of HEOs, made a huge contribution to excellent catalytic thermal stability at high temperatures. However, the sintering of noble metals usually occurred over traditional metal oxides, resulting in their unsatisfactory catalytic performance. Furthermore, the more elaborate structure between noble metals and HEOs for CO oxidation was characterized by X-ray absorption near edge structure spectra. Xu et al.²⁷ reported an advanced strategy to effectively combine Pd with (CeZrHfTiLa)_x (Pd₁@HEFOs) in the form of single atoms by mechanical milling. Fourier-transformed *k*³-weighted EXAFS (Figure 7F) illustrates the existence of isolated Pd^{x+} (0 < *x* < 2) species. Not only were single Pd atoms generated over Pd₁@HEFO but also the Pd₁@HEFOs afforded the optimized lattice oxygen species over that of the traditional Pd@CeO₂ catalyst, thereby exhibiting dramatically enhanced reactivity for CO oxidation at both the onset temperature (~80°C) and the complete temperature (~170°C). Likewise, the excellent CO conversion ability of Pd₁@HEFOs was enhanced by incorporation of Pd into the structure of HEFOs, as proved by the poor CO oxidation ability of the pure HEFO catalyst. These previous works have already validated the excellent stability of HEOs and noble-based HEOs for CO oxidation. Without exception, the Pd₁@HEFOs also exhibited outstanding stability of well-cycled measurement and the stability test at 170°C for CO oxidation (Figure 7F). As displayed above,⁶⁸ the HEOs catalysts showed potential for CO oxidation under harsh conditions owing to their excellent SO₂ resistance. However, except for SO₂, H₂O is also inevitable in vehicle exhaust. Surprisingly, Pd₁@HEFOs-HA retained stable physicochemical properties even through hydrothermal treatment. More important, Pd₁@HEFOs could effectively catalyze CO, C₃H₆, and NO through oxidation reactions. It is observed that the strong metal support interaction emerges when combining noble metals with HEOs, and the interaction endows noble metals-based HEOs with excellent CO catalytic performance under complicated conditions. This part also guides us in the precise preparation of a single-atom catalyst by virtue of the structure and property of HEOs, which is critical for further development in various kinds of catalytic fields.

CO₂ hydrogenation

To date, the tail control paths of CO₂ mainly include CO₂ capture, conversion, and utilization. Among them, the CO₂ conversion and utilization, especially CO₂ hydrogenation using a thermocatalytic route, could realize the generation of high-value-added products (such as alcohol and hydrocarbon) using CO₂ as the source. So far, the commercial CuZnAl catalyst has been widely applied into CO₂ hydrogenation

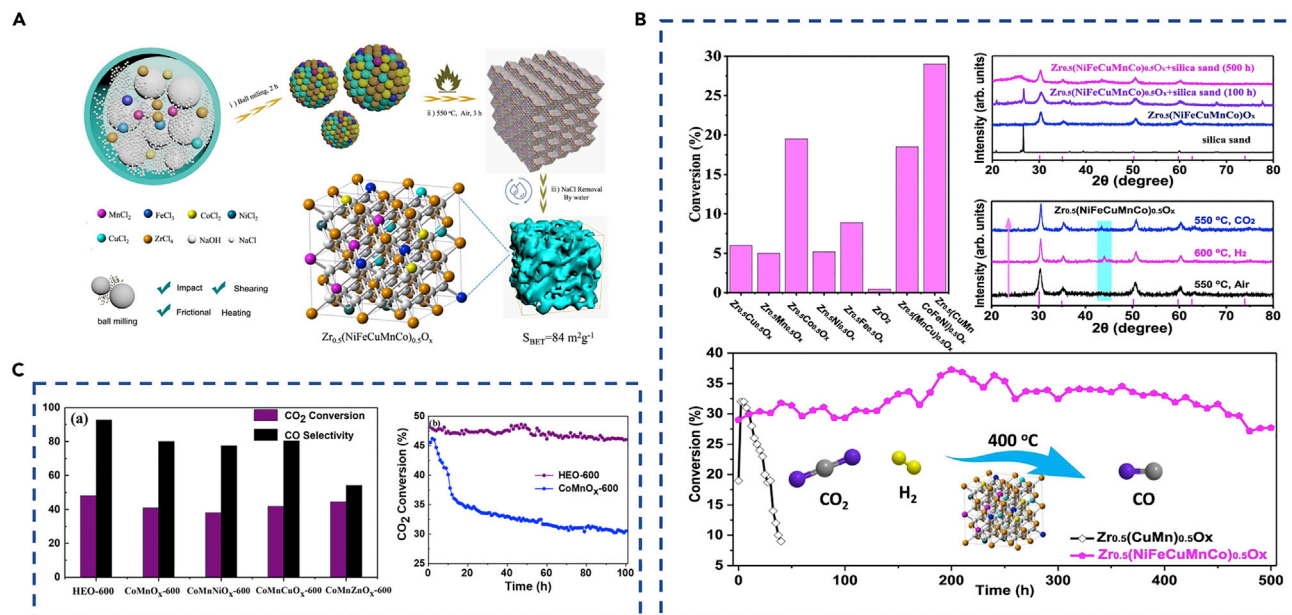


Figure 8. Preparation and structure of HEOs and application in CO₂ hydrogenation

(A) Preparation schematic of Zr_{0.5}(NiFeCuMnCo)_{0.5}O_x. Adapted with permission from Zhang et al.²⁸

(B) Left: Catalytic performance of Zr_{0.5}(NiFeCuMnCo)_{0.5}O_x and compared catalysts in CO₂ hydrogenation at 400 °C. Right: XRD patterns of reused Zr_{0.5}(NiFeCuMnCo)_{0.5}O_x after stability test. Bottom: Thermal stability of Zr_{0.5}(NiFeCuMnCo)_{0.5}O_x and Zr_{0.5}(CuMn)_{0.5}O_x in CO₂ hydrogenation. Adapted with permission from Zhang et al.²⁸

(C) Left: CO₂ hydrogenation activity of HEO-600 and counterparts under 500°C. Right: CO₂ hydrogenation stability. Adapted with permission from Zhang et al.⁷²

technology, but suffers from poor thermostability and selectivity. As demonstrated, the HEOs not only have mixed metal components, but also possess superior mechanical and thermal stability, thereby exhibiting huge potential in the CO₂ hydrogenation reaction with superior catalytic performance.

It is known that the HEOs have strong mechanical strength and superior thermostability, which could be effectively applied in the high-temperature thermocatalytic reaction. However, the common HEOs were prepared through co-precipitation or hydrothermal methods with small surface area and poor texture parameters, which is not beneficial to their catalytic performance. To address this issue, Zhang's group²⁸ designed cubic HEO Zr_{0.5}(NiFeCuMnCo)_{0.5}O_x using the mechanochemical method for CO₂ hydrogenation, as exhibited in Figure 8A. At first, five metal salts (Cu, Co, Ni, Fe, Mn) in the form of fluorides accompanied by ZrCl₄, NaOH, and NaCl were mixed through ball-milling for 2 h. Afterward, calcination and NaCl-removing treatments were used to obtain the final products. By adjusting the molar ratio of metal (nZr:nCu:nCo:nNi:nFe:nMn = 5:1:1:1:1:1) and calcination temperature (550°C), Zr_{0.5}(NiFeCuMnCo)_{0.5}O_x with high surface area (84 m² g⁻¹) was acquired. Moreover, the reduction treatment could enhance stability of structure and physico-chemical properties of Zr_{0.5}(NiFeCuMnCo)_{0.5}O_x under partly complicated conditions.

By comparison, it is obviously observed that Zr_{0.5}(NiFeCuMnCo)_{0.5}O_x exhibited higher CO₂ conversion than that of doped ZrO₂ catalysts (Zr_{0.5}M_{0.5}O_x, M = Cu, Mn, Co, Ni, Fe, CuMn) during CO₂ hydrogenation at 400°C. Meanwhile, almost no decline in CO₂ conversion at 400°C during the reaction over Zr_{0.5}(NiFeCuMnCo)_{0.5}O_x was observed in a span of 500 h (Figure 8B) due to thermal stability of the host structure. To summarize,

the unique physicochemical properties of HEO catalysts indeed promoted the thermal stability for their CO₂ hydrogenation reaction activity, which guided the design and preparation of metal-based catalysts, with improved catalytic activity and thermal stability for other reactions. Zhang et al.⁷² also obtained CuCoNi nanoalloys over the HEO Co₃MnNiCuZnO_x matrix through *in situ* generation to create the stable metal-oxide interface and applied for CO₂ catalytic conversion through the hydrogenation route. In this work, the structure of the obtained Co₃MnNiCuZnO_x is in a pure spinel phase with reversible characteristics. Meanwhile, CuCoNi alloys were generated by virtue of the entropy-driven force under reductive and oxidative recycles. The derived HEO-600 (600 is the calcination temperature) catalyst exhibited both higher CO₂ conversion and CO selectivity than that of CoMO_x-600 (M = Mn, MnNi, MnCu, MnZn) catalysts (Figure 8C). Predictably, the restriction of CuCoNi alloys phase over the Co₃MnNiCuZnO_x matrix could maintain long-term thermal stability (>100 h) at high temperatures (Figure 8C), further proving that HEO structure and physicochemical properties could motivate the design of an efficient catalyst for CO₂ hydrogenation with sintering-resistant ability.

According to the above discussion, it is widely acknowledged that the existing multifarious transition metal elements and superior structural stability of HEOs contribute to good catalytic performance with excellent thermostability. However, the pure constitution of transition metal oxides could not contribute to the optimal catalytic performance. Therefore, noble metals were introduced with transition metal oxides to further enhance their catalytic performance. Unfortunately, the sintering and agglomeration of noble metal-based catalysts under high temperatures easily resulted in poor stability. To solve this problem, the noble metals and HEOs were well combined to design highly efficient and stable gas-solid heterogeneous catalysts for the CO₂ hydrogenation reaction, as listed below.

In general, the high-temperature calcination process is essential for the generation of HEOs. Obviously, this strategy to prepare the noble-doped HEOs would bring about the sintering and agglomeration of noble metals. On these grounds, Mori et al.⁷³ proposed a strategy to directly obtain high entropy alloy (HEA) nanoparticles on the TiO₂ support by the hydrogen spillover effect (Figure 9A). During the process, the Pd-H species was generated through the partial reduction of Pd²⁺ to Pd nuclei under an H₂ atmosphere (step 1). Afterward, the reduction of Ti⁴⁺ to Ti³⁺ accompanied by transferred H atoms from the Pd nuclei (step 2) and the migration between the electrons of Ti³⁺ ions and the adjacent Ti⁴⁺ ions collectively promote the transfer of protons from the Ti⁴⁺ ions to O₂⁻ anions (step 3). As a result, the metallic species were rapidly reduced due to the presence of the moved H atoms over the TiO₂ surface (step 4) simultaneously, further regenerating Ti⁴⁺. Notably, the Pd-based HEAs could be formed at only 400°C. When applied for CO₂ hydrogen, it is obviously found that the CoNiCuRuPd/TiO₂ showed much higher yields of hydrogenated products (especially CH₄) than the same active content using MgO and Al₂O₃ as supports. As for the Pd/TiO₂ catalyst, almost no CH₄ yields and few higher CO yields were observed in the same conditions, suggesting that the HEA nanoparticles on TiO₂ could simultaneously improve their catalytic performance and selectivity. In addition, CoNiCuRuPd/TiO₂ exhibited much lower activation energy (37.7 kJ mol⁻¹) than that of Pd/TiO₂ (44.2 kJ mol⁻¹). More than that, the Pd/TiO₂ exhibited a gradual decline in CO₂ conversion with prolonging time, with a reduced factor of 0.76 in a span of 72 h, which was much lower than that of CoNiCuRuPd/TiO₂ (0.96) in the same conditions (Figure 9B).

Except for the experimental results, the catalyst with high entropy structure for CO₂/CO reduction was also combined by DFT calculation. For example, Pedersen et al.⁷⁴

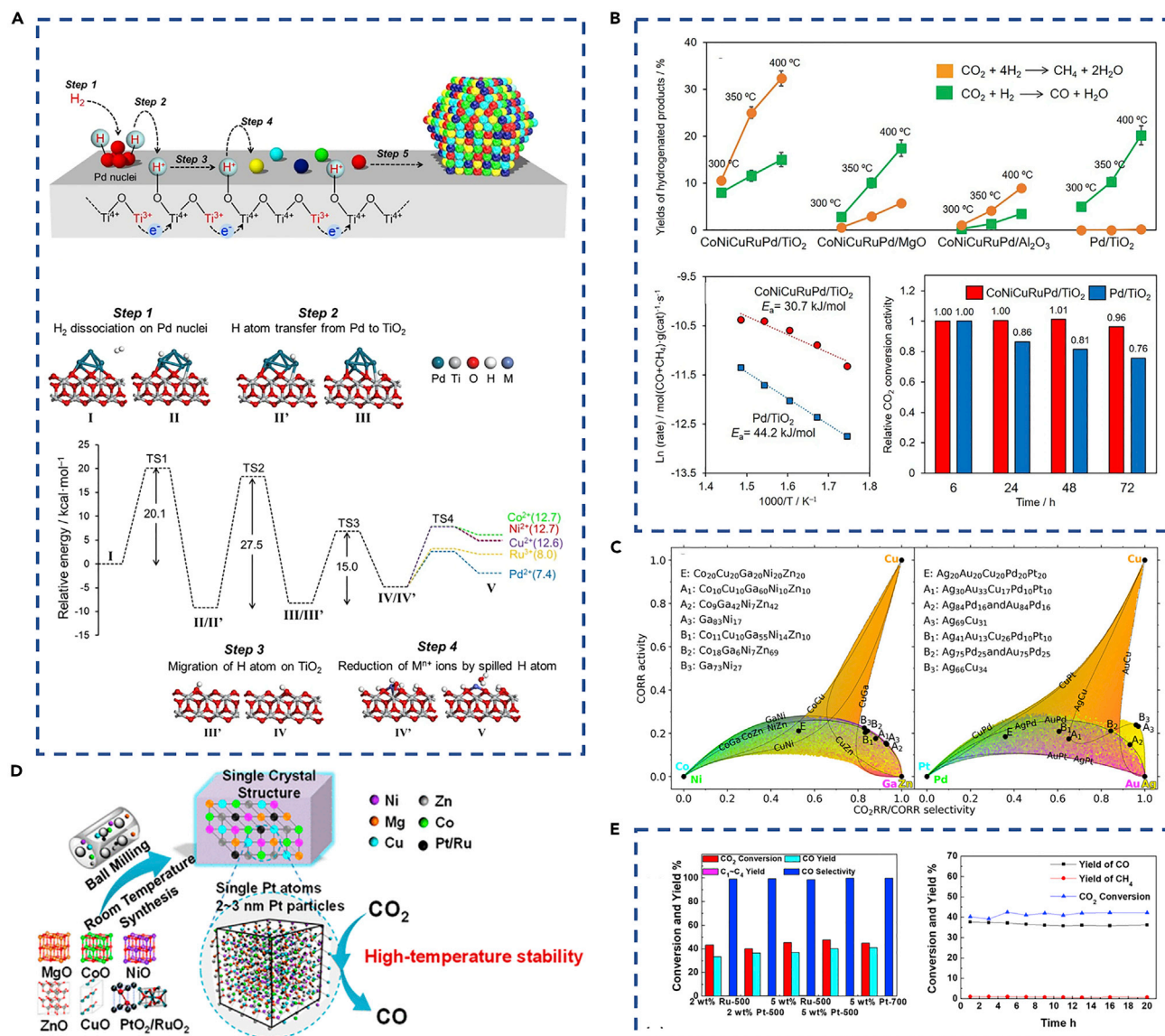


Figure 9. Preparation and structure of derived HEOs and application in CO₂ hydrogenation

(A) Schematic of the elementary steps on the $\text{TiO}_2(101)$ from DFT calculation. Adapted with permission from Mori et al.⁷³

(B) Top: Yields of hydrogenated products over different catalysts. Bottom: Arrhenius plots and relative stability activities over CoNiCuRuPd/TiO₂ and Pd/TiO₂ during CO₂ hydrogenation. Adapted with permission from Mori et al.⁷³

(C) Selectivity-activity plots over CoCuGaNiZn and AgAuCuPdPt for CO₂RR/CORR (RR, reduction reaction) selectivity and CORR activities. Adapted with permission from Pedersen et al.⁷⁴

(D) Mechanochemical synthesis of Pt/Ru-(NiMgCuZnCo)O catalysts. Adapted with permission from Chen et al.²⁹

(E) Left: CO₂ hydrogenation activity of different catalysts. Right: Stability over 5 wt% Pt-500 for CO₂ hydrogenation. Adapted with permission from Chen et al.²⁹

presented a framework of CoCuGaNiZn and AgAuCuPdPt for the reduction reaction of CO₂ and CO (CO₂RR and CORR). The optimal disordered alloy compositions were optimized to explore the effect of composition effects on the distribution of adsorption energies for the formation of H₂ as well as reduced CO (Figure 9C). As a result, only combining Cu species with GaNi to generate a catalyst can demonstrate perfect catalytic performance for CO₂RR/CORR and exhibit high yields of reduced carbon products. Furthermore, theoretical simulation was used to predict disordered alloys' valid catalyst

candidates from HEOs for optimal catalytic performance of CO₂ hydrogenation. Chen et al.²⁹ reported that there is a similar case of a combination mode of noble metals and HEOs. They used the mechanochemical synthesis method to obtain (NiMgCuZnCo)O at room temperature. Meanwhile, noble metal (up to 5 wt %) was introduced into (NiMgCuZnCo)O through ball-milling to attain a pure crystal structure with single Pt atoms and nanoparticles (2–3 nm) (Figure 9D). Subsequently, all of the Ru/Pt-based (NiMgCuZnCo)O catalysts with different noble metal content produced considerable CO₂ conversion (>~40%) with high CO selectivity (>95%) for CO₂ hydrogenation at 500°C. Even through a long-time test, both the CO₂ conversion and CO selectivity remained stable at a high level (Figure 9E). Different with the traditional noble loading way (e.g., impregnation), the introduction of noble metal into HEOs using hydrogen spill-over effect or direct ball-milling method could put these elements in a single crystal structure. As a result, the high reaction temperature could not cause the sintering of active species over the noble metal-based HEOs, consequently guaranteeing their considerable catalytic efficiency for CO₂ hydrogenation.

Other thermocatalytic reactions

With maximized configurational entropy and excellent structure stability, HEOs generate abundant catalytically active sites among different constituents and demonstrate an excellent catalytic performance for CO oxidation and CO₂ hydrogenation. Moreover, HEOs also could exhibit potential performance in various kinds of catalytic reactions by adjusting the structure and composition. For example, Deng et al.⁷⁵ prepared HEO MoNiCuZnCoO_x under different temperatures with stable and well-dispersed Mo species. The obtained MoNiCuZnCoO_x catalysts were used in oxidative desulfurization (dibenzothiophene) through a solid-liquid reaction. As shown in Figure 10A, the sulfur-containing compound was completely and quickly converted over HEO-900 (3 h) and HEO-1000 (3.5 h) at 120°C, while slightly more than half of the sulfur (58%) was removed over HEO-800 after 4 h in the same condition. That is because the suitable high temperature could guarantee the optimization of the entropy effect for highly dispersed metal elements, boosting the catalytic performance remarkably. Meanwhile, Li et al.⁷⁶ prepared a denary multi-element oxide (MEO) catalyst (Figure 10B). Compared with the temperature-driven and oxidation-driven effects, the entropy-driven process by introducing more elements to guarantee the organic combination of noble metals and MEOs is easy to complete. The obtained (Zr,Ce)_{0.6}(Mg,La,Y,Hf,Ti,Cr,Mn)_{0.3}Pd_{0.1}O_{2-x} exhibited superior mechanical property and excellent structural stability. As a result, it also displayed much better catalytic stability of methane combustion than those of (Zr,Ce)_{0.6}Mg_{0.3}Pd_{0.1}O_x and PdO_x.

Furthermore, HEOs present application potential for important compound decomposition and dehydrogenation reactions. Zhai et al.³¹ proposed a concept to prepare polycation oxides (PCOs, marked as (FeMgCoNi)O_x) using the sol-gel technique to obtain H₂ through two-step thermochemical water splitting (TWS) (Figure 10C). In detail, the metal ions of (FeMgCoNi)O_x were in the form of rock salt and spinel phases, and could swing without a complete transition during two-step TWS between high temperature (T_H) and low temperature (T_L). Consequently, the (FeMgCoNi)O_x could realize the effective and undivided decomposition of H₂O to H₂ at low T_H (<1,100°C) without H₂ oxidation at T_L. Surprisingly, the as-obtained H₂ yields over (FeMgCoNi)O_x catalyst given higher times (~45) than that of CeO₂ and spinel ferrites at different conditions (Figures 10D and 10E). More important, the H₂ production efficiency is much better than that of CeO₂ or spinel ferrites at mild conditions (T_H = 1,100°C), which demonstrates superior performance of suppressing H₂ oxidation during water splitting. It is believed that the special structure

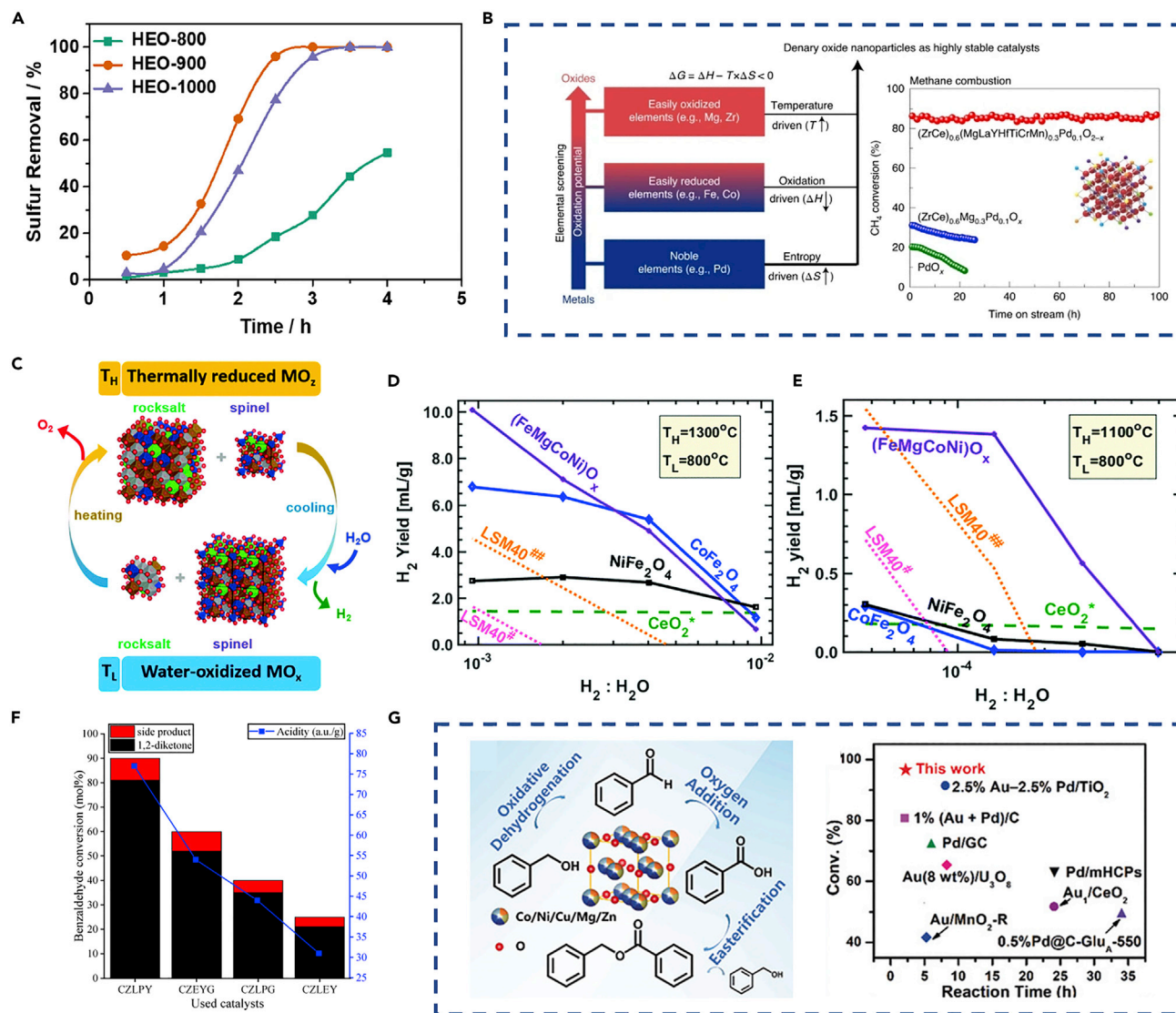


Figure 10. HEOs for other classical thermocatalytic reactions

(A) Sulfur removal over the as-obtained HEOs catalysts. Adapted with permission from Deng et al.⁷⁵

(B) Left: Synthesis diagram of single-phase MEO nanoparticles. Right: Catalytic stability of different catalysts in terms of CH₄ conversion. Adapted with permission from Li et al.⁷⁶

(C) Schematic of two-step TWS. Adapted with permission from Zhai et al.³¹

(D and E) Thermochemical water splitting performance over FeMgCoNi)O_x, CeO₂, and perovskite LSM40. Adapted with permission from Zhai et al.³¹

(F) Catalytic ability of the different HEOs for benzaldehyde reaction. Adapted with permission from Tatar et al.⁷⁷

(G) Left: The reaction pathway of benzyl alcohol oxidation over holey lamellar HEOs catalyst. Right: Catalytic conversion of holey lamellar HEOs catalyst with reported catalysts. Adapted with permission from Feng et al.³²

and physicochemical properties of HEOs could also contribute to H₂ production through water splitting.

In addition to gas-solid catalytic reactions, HEOs possess the potential for solid-liquid reactions. Tatar et al.⁷⁷ designed Ce-Zr-based HEO catalysts for catalyzing aldehydes to 1,2-diketones (Figure 10F). By optimizing reaction conditions, it is demonstrated that CZLPY (Ce_{0.2}Zr_{0.2}La_{0.2}Pr_{0.2}Y_{0.2}O₂) exhibited the highest activity, which was promoted by the organic incorporation of various cations into the HEO structure and derived unique physicochemical properties. Due to the good

synergistic effect of Ce, Zr, La, Pr, and Y in one crystal structure in CZLPY, excellent and stable catalytic conversion of aldehydes to 1,2-diketones was completed relatively painlessly. Moreover, Feng et al.³² prepared holey lamellar HEOs of the $\text{Co}_{0.2}\text{Ni}_{0.2}\text{Cu}_{0.2}\text{Mg}_{0.2}\text{Zn}_{0.2}\text{O}$ catalyst through an ordinary anchoring and merging process for benzyl alcohol oxidation without solvent and oxygen. With a mesoporous structure, the obtained $\text{Co}_{0.2}\text{Ni}_{0.2}\text{Cu}_{0.2}\text{Mg}_{0.2}\text{Zn}_{0.2}\text{O}$ catalyst realized highly efficient generation of benzoic acid or benzaldehyde by adjusting reaction conditions (Figure 10G). Encouragingly, the superior catalytic performance (>98% conversion) using these HEOs was obtained only at 120°C for as low as 2 h—much better than most reported catalysts (Figure 10G), which promoted by the holey lamellar framework together with abundant oxygen vacancies over the $\text{Co}_{0.2}\text{Ni}_{0.2}\text{Cu}_{0.2}\text{Mg}_{0.2}\text{Zn}_{0.2}\text{O}$ catalyst. To summarize, it is believed that the good synergistic effect of different metal elements in the HEOs offers outstanding guidance in designing efficient heterogeneous catalysts for both gas-solid and liquid-solid phases.

Electrocatalysis

In addition to thermocatalysis reactions, the electrocatalysis reaction, as a sustainable development path, plays a more and more important role in efficient energy conversion and storage.^{78–81} Some important electrocatalysis reactions, such as water to produce H_2 ,^{82,83} N_2 reduction to synthesize NH_3 ,^{84,85} CO_2 reduction to small organic molecules,^{86,87} electrooxidation of glucose,⁸⁸ and other organic substances to high-value chemicals,^{89,90} which affects many aspects of our being. Undoubtedly, the electrocatalyst is the key object to achieve the above electrochemical conversion with high selectivity, high activity, and excellent stability.^{91,92} Similarly, the entropy effect also plays a vital role in electrocatalysis, reflected in that the multiple synergistic effect breaks the scaling relationships for electrocatalysis and realizes the optimal binding energy of the reacting species and the catalyst.^{9,24} Interface control, stress strategy, and defect engineering methods optimize the electronic structure and morphology characteristics of HEOs, providing abundant catalytic active sites and stable catalytic configurations, thus exhibiting excellent electrocatalytic activity and stability.^{93–95} Next, we reviewed comprehensively the key applications of HEOs in electrocatalysis such as the oxygen evolution reaction (OER), the oxygen reduction reaction (ORR), the electrooxidation reaction, and the Li-S battery catalysis in recent years, and elaborately discussed the relationship between the structure of the analysis material and the optimization of catalytic activity.

Oxygen catalysis

OER

The OER is a four-proton coupled electron transfer process with slow kinetics, which is considered to be the decisive step that limits the overall efficiency of H_2 production and the rate of energy conversion.^{96–98} IrO_2 and RuO_2 are acknowledged to be the benchmark catalysts for OER due to their ideal initial performance.^{99,100} However, scarce reserves, high cost, and poor stability of these catalysts limit the extensive development of energy-conversion devices.^{101,102} Efficient OER catalysts are essential for large-scale H_2O electrolysis to produce H_2 , metal-air batteries, and other energy conversion and storage.^{103–105} Among many potential alternative catalysts, perovskite oxides have been widely studied due to their high activity, diverse structure, and flexible composition.^{106,107} Recently, HEPOs could be precisely controlled to improve their electronic structure for promoting the generation of multiple catalytic active sites, increasing the electron transmission rate of the catalyst, and further expanding the application of perovskite oxide materials in OERs.^{108–110}

HEPOs are one effective class of key catalysts for improving the catalytic activity and stability of OERs, creating lattice defects, and exposing active sites by introducing

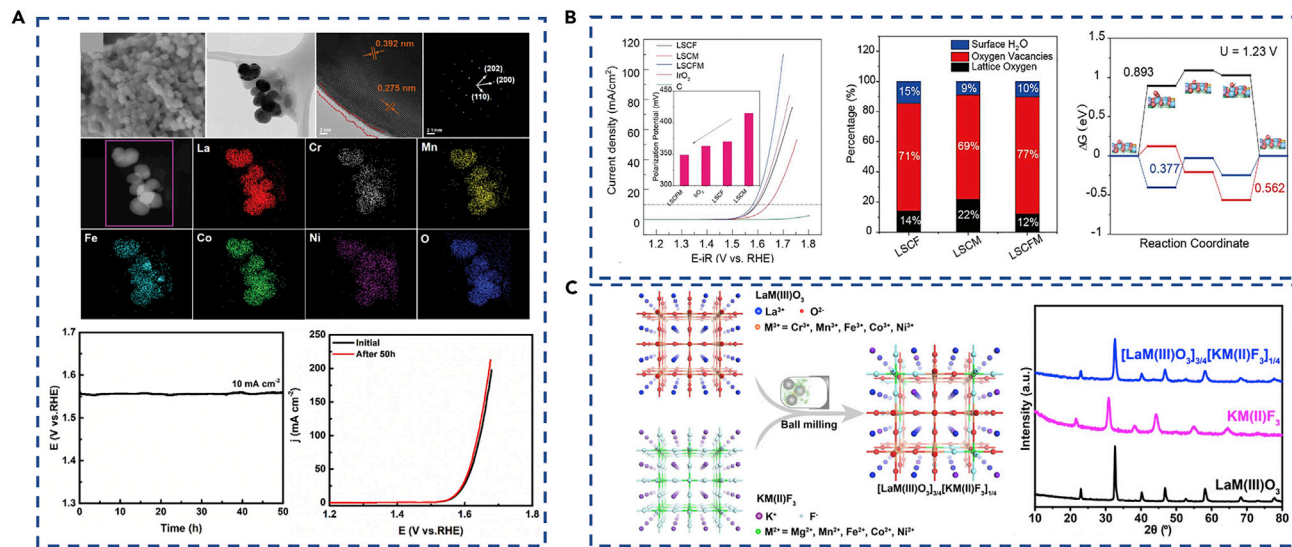


Figure 11. Preparation and structure of HEOs and application in OER

(A) Morphological characteristics of HEPOs after OER test (SEM, TEM, high-resolution TEM [HRTEM], selected area electron diffraction [SAED], and scanning TEM [STEM] mapping), and electrochemical stability test curve for 50 h. Adapted with permission from Ting et al.¹⁰⁸

(B) Linear sweeping voltammogram (LSV) for OER, the ratio percentage of different oxygen species, and calculated free energy diagram of LSCFM and other samples. Adapted with permission from Sun et al.¹⁰⁹

(C) Synthetic diagram and XRD patterns of perovskite oxide-fluoride solid solution. Adapted with permission from Dai et al.¹¹⁰

multiple metals. For instance, Ting and colleagues¹⁰⁸ proposed a type of lanthanum-based HEPO catalyst for OER, adopting a simple co-precipitation method to prepare uniform HEPO nanoparticles of the B-sites lattice are Cr, Mn, Fe, Co, and Ni first-row transition metals. The experimental results show that high Co content in these HEPOs can significantly enhance the activity of OER as the active center. At the same time, the role of multi-component elements, such as high oxidation state elements (Cr⁶⁺, Mn⁴⁺, Fe³⁺, and Co³⁺) and oxygen vacancies caused by adjusting the ratio of Mn elements, cannot be ignored. The stability of HEPO catalyst is reflected by the morphology characterization map and electrochemical data after long-term cycling (Figure 11A). After 50 h of continuous electrolysis, the potential signal and polarization curve did not change significantly, exhibiting stable catalytic performance. Scanning electron microscopy (SEM) and transmission electron microscopy (TEM) images verified that the morphology of the sample was stable after continuous electrolysis, showing a uniform and highly dispersed state. Furthermore, it is theoretically verified that the catalyst follows the adsorption evolution mechanism (AEM) reaction path, which is consistent with the experimental results. In addition, the OER mechanism can be effectively transformed from AEM to the lattice oxygen mechanism (LOM) by adjusting the oxygen vacancy concentration in the HEPO material. Sun et al.¹⁰⁹ presented perovskite cobaltate (La_{0.6}Sr_{0.4}Co_{0.8}Fe_{0.1}Mn_{0.1}O_{3-δ}, LSCFM) nanofiber electrocatalysts to mediate OER in the alkaline environment with high activity and good stability. As presented in Figure 11B, it was disclosed that LSCFM presented rich surface oxygen vacancy concentration and ultra-fast oxygen ion diffusion velocity when compared with a single dopant. Both experimental and theoretical calculation results further explained that the formation of reactive lattice oxygen sites promoted the OER kinetic process, demonstrating the effectiveness of the configurational entropy effect. Furthermore, the combination or hybridization of oxides and halides to form both multi-anionic and multi-cationic solid solutions, with distinctive metal ion sites and synergistic properties, is expected to surpass traditional perovskite catalysts. Dai et al.¹¹⁰ synthesized a solid solution of perovskite oxide and fluoride

$\text{La}(\text{CrMnFeCoNi})\text{O}_{33/4}\text{K}(\text{MgMnFeCoNi})\text{F}_{31/4}$ with a single-phase crystal structure, a high degree of mixing, and uniform element distribution through mechanochemical methods (Figure 11C). The high-entropy solid solution exhibited excellent OER activity and stability in alkaline electrolytes, exceeding the current best perovskite catalysts owing to optimized components and electronic structure. So far, the design strategy of HEO oxygen evolution catalysts lies mainly in its tunable lattice parameters, element composition, and electronic structure, which is helpful to optimize the energy absorption. Nevertheless, the optimization of multi-element electronic structures is essential to improve catalytic activity and stability. However, HEOs are used mostly in alkaline media thus far. To demonstrate the intrinsic stability of HEOs, the development of corrosion-resistant OER catalysts is expected to solve the poor stability in acidic media, and realize the high efficiency and economic benefits of proton exchange membrane devices.

ORR

ORR and OER processes are the basic components of metal-air batteries.^{111,112} The complex and slow-kinetic four-electron transfer process hinders the reaction rate, thereby limiting the conversion efficiency of metal-air batteries.^{113,114} For ORR, it is of sustainable significance to design low-cost, efficient, and stable materials to replace scarce Pt catalysts for the wide-ranging applications of energy equipment.^{115–117} Similar to OERs, the HEOs with adjustable structures and multi-component space also show excellent oxygen oxidation performance.^{15,33,118,119} More specifically, mixed cation sites can effectively interact with various intermediate species to improve intrinsic activity, and the entropy stabilization effect contributes to long-term stable operation. For example, Hu et al.¹¹⁹ used a far-equilibrium strategy enabled by electrical joule heating of carbon materials to synthesize uniformly 10-element ($\text{Hf,Zr,La,V,Ce,Ti,Nd,Gd,Y,Pd}$) O_{2-x} HEO (10-HEO) nanoparticles dispersed on a commercial carbon powder substrate. As displayed in Figure 12A, the high temperature and rapid synthesis feature avoid the enrichment and agglomeration of HEO nanoparticles during the synthesis process, improving the structural stability of the catalyst by virtue of a highly dispersed state, single-phase structure and strengthening the interaction between the nanoparticles and carbon support. The 10-HEO catalyst showed a half-wave potential ($E_{1/2}$) at 0.85 V versus the reversible hydrogen electrode (RHE) and the stability of current attenuation by 14% after 100 h of operation, preceding other comparative samples. After detailed analysis, Hu et al. found that the oxidation state of Pd contributed to the enhancement of ORR activity as the main active sites, as did oxygen deficiency and multi-element synergy. Surface oxidation modification of HEA materials results in the HEO catalyst with mixed entropy effect showing outstanding performance. In this case, Qiu et al.³³ proposed a dealloying method to form uniform spinel-type oxides on the surface of HEA materials. For instance, an equal proportion of AlNiCoRuMo single solid solution phase spontaneously forms multi-component spinel oxide through the alkali corrosion process, showing impressive ORR and OER performance. In Figure 12B, as dual-function air electrodes, the material exhibits excellent charge-discharge cycle durability of more than 500 h, which is suitable for high-current and deep charge-discharge/charge, suppressing the commercial Pt/C-IrO₂-based battery. Furthermore, it is theoretically and experimentally demonstrated that the synergistic combination of multi-components in a single phase can induce the five elements to produce complex electronic interactions and generate abundant active sites, outperforming the binary and ternary systems. Not only that, HEOs are also an excellent multifunctional carrier for anchoring metal nanoparticles, clusters, or single atoms, strong interaction stabilizing the active atoms, providing a novel platform of creating combinatorial materials. Therefore, Qiu et al.¹⁵ also used the chemical

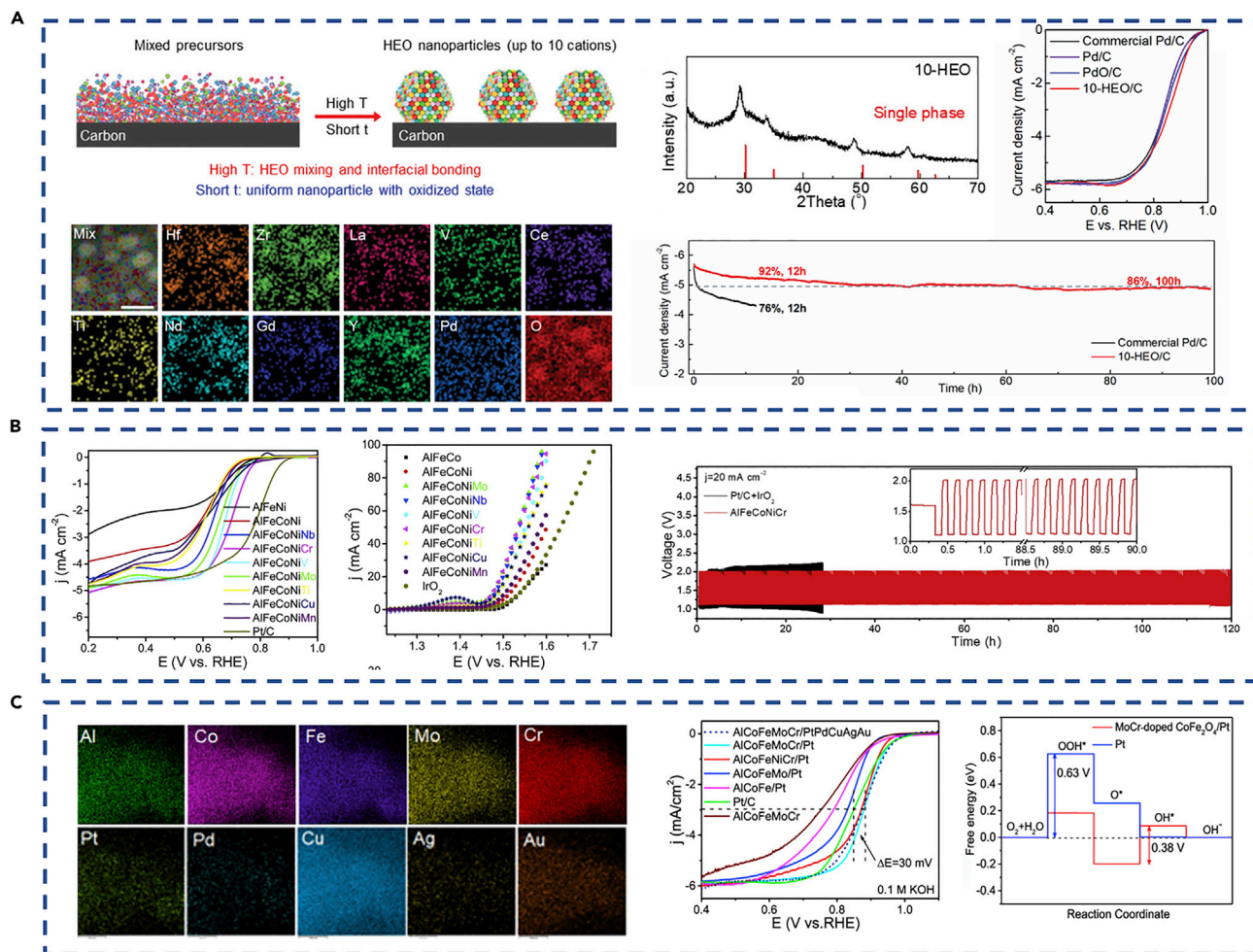


Figure 12. Preparation and structure of HEOs and application in ORR and Zn-air battery

(A) Left: Schematic of the preparation of 10-HEO nanoparticles and their elemental mappings; Right: XRD patterns and ORR activity and stability diagram. Adapted with permission from Hu et al.¹¹⁹

(B) The polarization curves of ORR and OER and diagram of liquid Zn-air battery for long-time cycling test. Adapted with permission from Qiu et al.¹¹⁸

(C) The STEM-energy-dispersive X-ray spectroscopy (EDS) mapping of AlCoFeMoCr/PtPdCuAgAu composite, ORR polarization, and free energy diagrams for AlCoFeMoCr/Pt and comparison samples. Adapted with permission from Qiu et al.¹⁵

dealloying method to synthesize highly dispersed Pt nanoparticles anchored on the AlCoFeMoCr HEO carrier, showing the uniform distribution of metal clusters in the rugged HEO support of 10 elements. After the addition of trace Pt (~4 wt %) into HEOs, the half-wave potential shifted 30 mV, obviously surpassing the electrocatalytic activity of commercial Pt/C. The first-principles calculations analysis showed that the enhancement of bifunctional catalytic activity originated from the synergy and electron transfer between nanoporous HEO (np-HEO) and Pt, which adjusts the intermediate adsorption energy to improve the activity. Later, they¹²⁰ loaded different amounts of Ag metal on the surface of (AlNiCoFeCr)₃O₄ by the same method, achieving bifunctional OER and ORR activities. It is important to note that Ag modification affects the electronic structure of Co in the active center, and the electron transfer effect optimizes the adsorption energy of the intermediate species. From the above findings, one can conclude that HEOs with abundant defects on the surface and stable structure, multi-element synergistic catalytic effects, and stable carriers anchoring the active metal sites could effectively promote catalytic

activity and stability. Specifically, the coordination environment of the metal active site and bonding mode with the complex components of HEO carriers are crucial for understanding the mechanism and developing *in situ/operando* characterization techniques and theoretical systems.

Electrooxidation

Organic oxidation

The electrochemical conversion of organic substances (e.g., ethanol, urea, glucose) into fuels and high-value-added chemicals to efficiently and environmentally friendly replace traditional fossil energy plays a pivotal role in the energy supply.^{121–124} For example, the catalytic oxidation of 5-hydroxymethylfurfural to 2,5-furandicarboxylic acid (FDCA) is promising to replace petroleum-derivative terephthalic acid to produce renewable polymers.^{125,126} The HEOs with stable entropy effects also have wide application potential in the catalytic oxidation of organic matter. For instance, Wang et al.⁹⁵ synthesized HEO nanosheets (FeCrCoNiCu)₃O₄ with abundant oxygen vacancies through a low-temperature plasma sputtering strategy (Figure 13A). Compared with the HEOs synthesized by the reverse co-precipitation method, the low-temperature plasma method shows obvious advantages, which are reflected in Figures 13B and 13C: (1) the material's low crystallinity, high specific surface area, and porous characteristics optimize the electrochemical mass transfer rate; and (2) the high surface roughness and rich oxygen defect properties of the material expose the active center, improving the catalytic activity. The electrochemical measurements (Figure 13D) show that this material has significantly improved current response, low onset potential (1.35 V versus RHE), high current density, and conversion efficiency (~100%), verifying that the abundant oxygen vacancies on the surface can intensify the intrinsic activity of HEOs. Therefore, it is indicated that HEOs have the potential for electrochemical biomass conversion, further extending to glucose oxidation, lignin conversion, and alcohol oxidation.

Inorganic oxidation

Electrooxidation of inorganic substances (e.g., H₂, hydrazine hydrate, NH₃) provides power for fuel cells, which has the advantages of large capacity, high specific energy, high conversion efficiency, and wide power range.^{127–129} For a mild and safe ammonia oxidation reaction (AOR), in terms of thermodynamics and kinetics, the operating potential of the catalyst must be lower than thermodynamic ORR potential and overcome the loss of electrons to achieve a high transfer rate.¹²⁷ Liu et al.³⁴ designed high-entropy spinel-type oxides (Mn,Fe,Co,Ni,Cu)₃O₄ using layered double hydroxide as a precursor for the AOR catalyst (Figure 14A). The high entropy effect can not only disperse each metal cation to form a uniform solid solution and expose more sites but also adjust the center of the *d*-band to achieve the best adsorption energy. The single-phase crystal structure and uniform element distribution characteristics of HEOs are shown in Figure 14B. Notably, the resultant HEOs as multi-component catalysts exhibit a high nitrogen production rate of 7.2 mmol mg⁻¹ s⁻¹ and over 90% Faraday efficiency (FE) at 1.0 V versus normal hydrogen electrode (NHE) (Figure 14C), which is compatible with activating the N–H bond and promoting the desorption of N–N species on the catalyst surface.

The electrocatalytic oxidation technology of organic and inorganic substances at the preliminary stage of development is an important way to realize energy conversion and sustainable development. The rise of stable HEOs with adjustable components has injected new dynamics into the design of electro-oxidation catalysts, which is conducive to activating each active site to achieve the series catalysis of reactants.

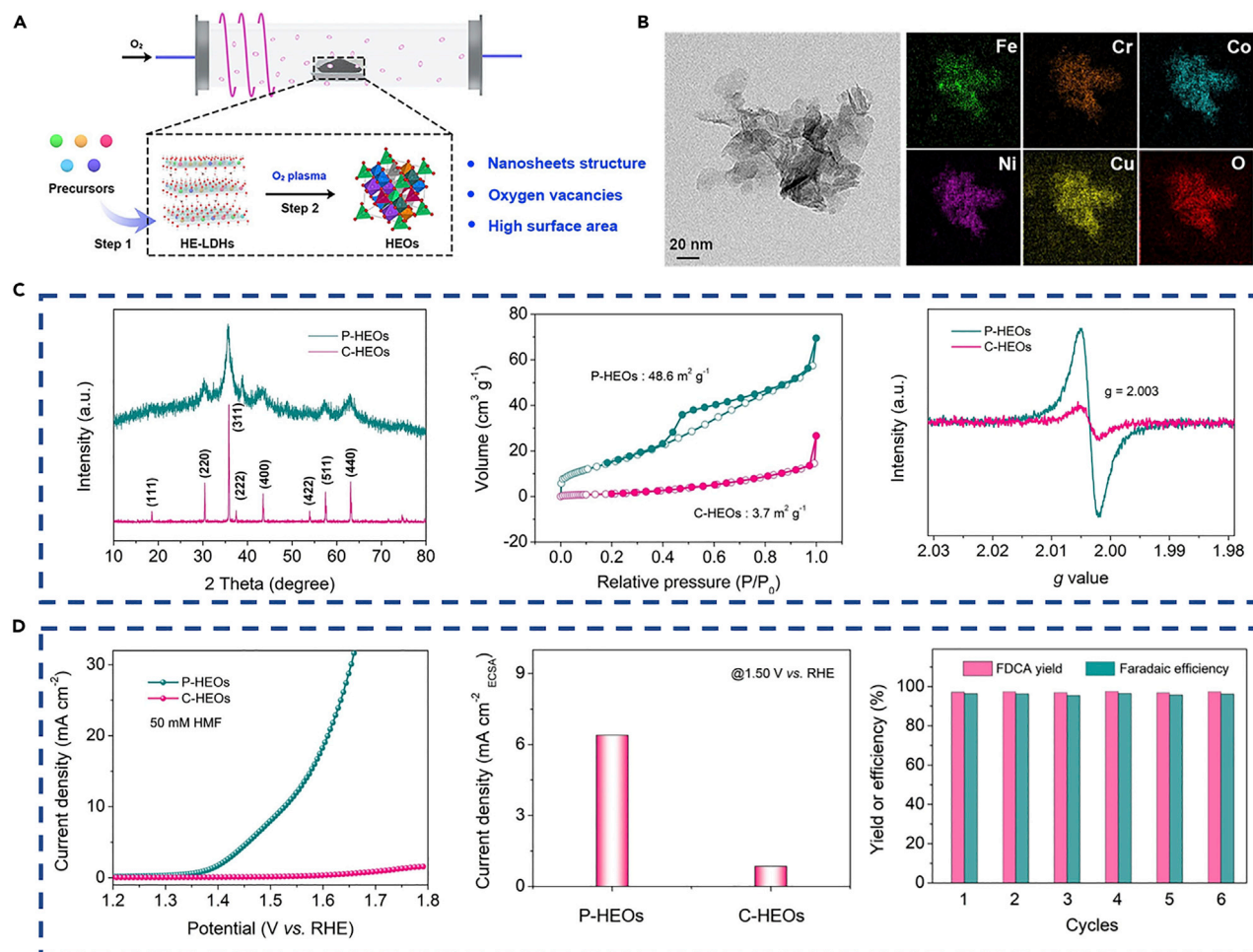


Figure 13. Preparation, structure of HEO catalysts application in 5-hydroxymethylfurfural oxidation reaction

(A) Schematic diagram of low-temperature plasma strategy for HEOs.

(B–D) TEM and EDX mapping images (B), (C) compositional characterization of the fabricated HEOs, XRD pattern, N₂ adsorption-desorption isotherms, and electron paramagnetic resonance (EPR) spectra, and (D) electrochemical results of HEOs, LSV curves, current density normalized by the electrochemically active surface area (ECSA), and FDCA yield and faradaic efficiency of HEOs. Adapted with permission from Wang et al.⁹⁵

Electrocatalysis in Li-S batteries

Li-S batteries are considered to be an energy storage system with broad application prospects due to the advantages of low cost, high theoretical capacity (1,675 mAh g⁻¹), high energy density (2,600 Wh kg⁻¹), and few safety hazards.^{130,131} For the cathode, the slow conversion process between insulating sulfur and Li₂S₂/Li₂S counteracts the efficient utilization and stability of active sulfur in lithium batteries.^{132–134} The insulating properties of sulfur and lithium polysulfides (LiPSs) and the shuttle effect of dissolving LiPSs are the bottlenecks for the development of Li-S batteries, inhibiting the practical application of Li-S batteries. Therefore, porous carbon materials, metal oxides, sulfides, conductive polymers, and other materials form a conductive network, expose abundant active sites, and prohibit the dissolution and diffusion of polysulfides to restrain the shuttle effect.^{135–139} It is worth noting that HEOs are one of the potential host materials of cathodes for Li-S batteries due to their intrinsic thermodynamic stability and metal conductivity. It is specifically embodied in (1) the abundant active sites randomly occupied by the multi-metal components that stabilize LiPSs; (2) the multi-component synergistic action that accelerates the adsorption and electrochemical conversion of Li₂S₆; and (3) the lattice

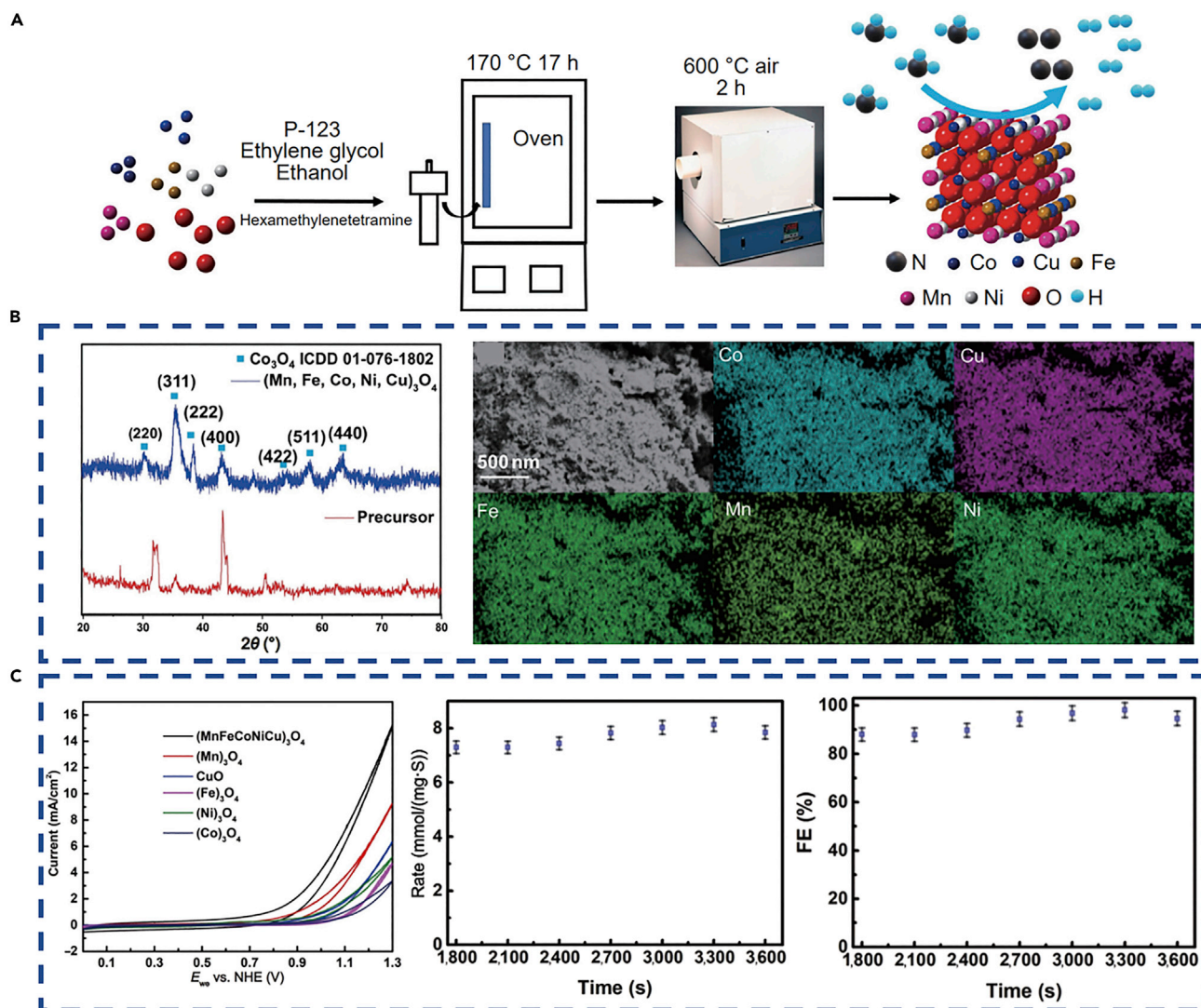


Figure 14. Preparation and structure of HEO catalyst and application in AOR

(A) Schematic representations of synthesis (Mn,Fe,Co,Ni,Cu)₃O₄.

(B) XRD patterns and energy-dispersive X-ray analysis (EDX) mapping for the as-obtained HEO.

(C) Electrochemical test of HEO, cyclic voltammetry polarization, N₂ evolution rate, and faradic efficiency of N₂. Adapted with permission from Liu et al.³⁴

distortion and charge compensation of HEOs for high electrons and ionic conductivity that improve the cycle stability and electron transmission of the working battery. As a typical example, Qiao et al.³⁵ proposed a strategy to inhibit the shuttle of polysulfides, using HEOs (Ni,Mg,Cu,Zn,Co)O as an immobilizing mediator to LiPSs (Figure 15A), which exhibits better battery performance than single metal oxides. The mechanism analysis results (Figure 15B) show that the interaction between the metal species in high-entropy metal oxides and LiPSs (the synergistic characteristics of Ni and S, Li, and O) significantly improves the sulfur retention characteristics of the material, which alleviates the shuttle effect of LiPSs and promotes the electrochemical conversion process with stable cycle performance. Similar results are also obtained from HEO ((Mg_{0.2}Mn_{0.2}Ni_{0.2}Co_{0.2}Zn_{0.2})Fe₂O₄) nanofibers as the catalytic host of sulfur.¹⁴⁰ In this work, high-entropy oxidized spinel nanofibers were synthesized by electrospinning, significantly promoting the transformation of soluble LiPS. It is indicated that a uniform single phase with high specific

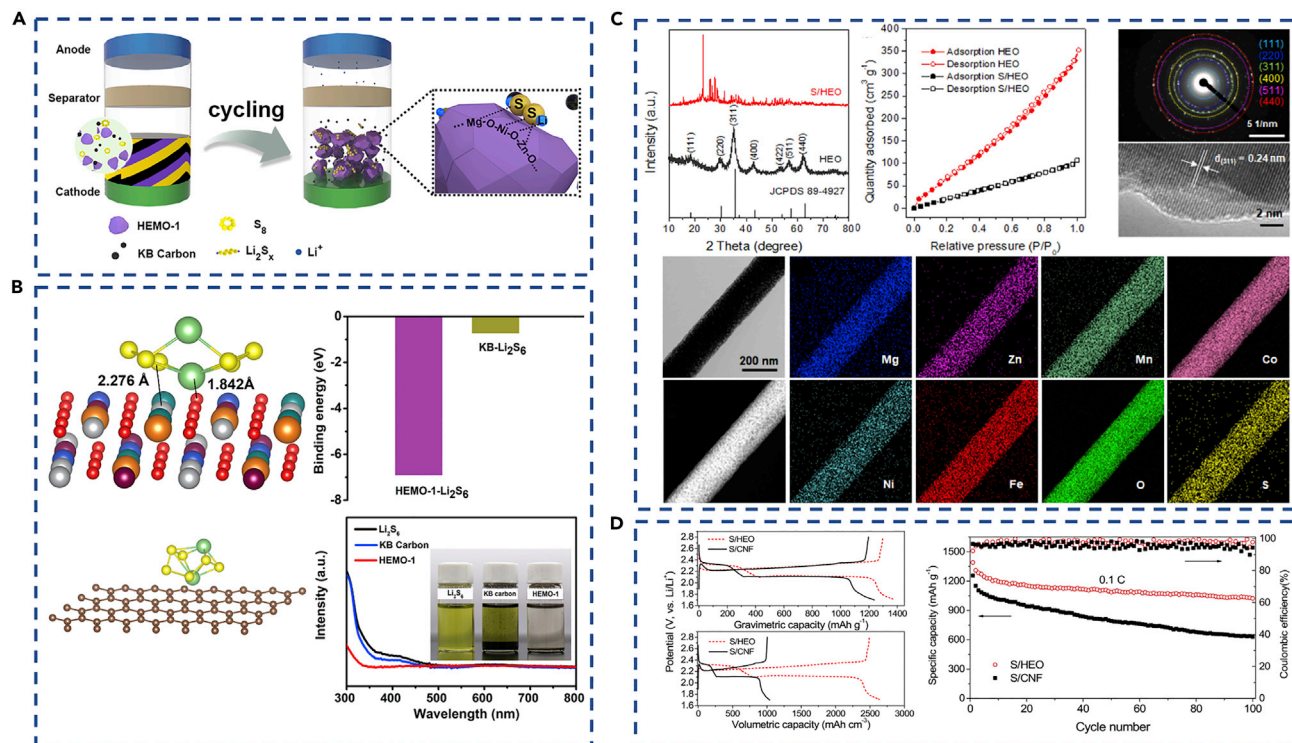


Figure 15. Structure characterizations of HEO catalyst for Li-S catalysis

(A) Schematic of cell configuration for Li-S battery.

(B) Geometry configuration of Li_2S_6 binding to HEMO or Ketjen black carbon, calculated binding energies of Li_2S_6 with HEMO and ultraviolet/visible absorption spectra of Li_2S_6 solution after the additives of HEMO and Ketjen black carbon. Adapted with permission from Qiao et al.³⁵

(C) Structural characterization of the fabricated HEO nanofibers. XRD patterns, N_2 adsorption-desorption isotherms, the corresponding SAED pattern, HRTEM image, HAADF-STEM image, and the EDS elemental maps.

(D) Electrochemical evaluation results for HEO nanofibers. The initial discharge/charge curves and cycle stability of Li-S batteries tested at 0.1 C rate. Adapted with permission from Gao et al.¹⁴⁰

surface area and the polymetallic elements are homogeneously distributed on the surface of the carbon nanofibers, achieving excellent electrocatalytic activity and cycle stability (Figure 15C). Based on the structural advantages of HEOs, the S/HEO composite material exhibits a high volumetric capacity of $2,627.9 \text{ mAh cm}^{-3}$ and a high tap density of 1.92 g cm^{-3} (Figure 15D), as well as excellent sulfur utilization and cycle stability, implying that the strong chemical binding of sulfur species to the HEO catalytic host limits the shuttle effect of LiPS. Moreover, HEOs effectively promote the redox kinetics process, enhance the Li-ion diffusion rate, and reduce the charge transfer resistance, thereby maintaining the highly reversible process of the sulfur cathode.

Overall, the concept of high configuration entropy is the key to achieve the high catalytic activity of the sulfur redox reaction with broad application prospects. Compared with a single metal compound, multiple metal compounds are more conducive to the preparation of polysulfide catalysis and conversion due to the synergy between different metal cations. Therefore, the modification of HEOs through interface control and defect engineering strategies can achieve highly reversible and long-term cycling Li-S batteries.

CONCLUSIONS AND OUTLOOK

The synthesis and analysis of the physicochemical properties and the catalytic applications (thermocatalysis and electrocatalysis) of HEOs have been summarized and

discussed. It is found that the original HEOs could be effectively applied for various kinds of catalytic reactions. In addition, the modification of HEOs and the combination of HEOs and noble metals could further optimize its catalytic performance. In particular, the strong mechanical strength and excellent thermostability would benefit HEO catalytic performance under harsh conditions, which expands its potential for industrial applications.

Despite the great progress made in HEOs for chemical catalysis, some challenging issues and future directions should be considered to further optimize its functionalized applications for both catalytic and other purposes, as listed below:

1. Innovative HEMs. There is an urgent need to develop novel synthetic strategies to prepare HEOs with a controllable morphology (e.g., 2D structure) and ultra-high specific surface areas for the exposure of active sites. For the conventional HEOs, some post-treatment strategies (e.g., acid etching) could be designed to precisely remove one or two metal elements in the framework to obtain HEOs with well-defined cation defects, thereby improving their physicochemical properties and catalytic performance. Furthermore, the oxygen vacancy and activated lattice oxygen could also be created through *in situ* modulation/post-treatment strategies to enrich their structural feature advantages. In addition, further expand the range of unknown HEMs (including but not limited to HECs, HENs, HEBs, and HEFs) for catalytic applications is necessary. Meanwhile, it is important to study the interaction between geometric electronic structure and physicochemical properties (e.g., strain, mechanical, magnetic, dielectric properties) of HEMs. High-throughput synthesis and screening of HEOs require the development of new concepts in catalyst design to address material challenges in renewable energy technologies, with the ultimate goal of efficient and environmentally friendly large-scale controlled preparation.
2. Advanced characterization. The development of advanced *in situ* characterization techniques is of great significance to enable in-depth study of HEOs catalyst states. At present, the analysis of catalytically active centers (defects, stress, and interfacial effects) is still difficult due to the complexity of the compositional structure of HEOs using traditional characterizations (e.g., X-ray photoelectron spectroscopy [XPS], Raman, and X-ray absorption fine-structure [XAFS] spectroscopy). Therefore, further development of characterization methods such as 3D atom probe tomography (3D-APT) and 4D electron energy loss spectroscopy (4D-EELS) to achieve ultra-high spatiotemporal resolution is essential for elucidating the microchemical structure of HEOs, and designing the establishment of structure-activity relationships in heterogeneous catalysis and revealing the catalytic mechanisms. Furthermore, the in-depth study of structural features and properties of HEOs through advanced characterizations could specifically guide their chemical catalysis reactions and development prospects.
3. Perfect theoretical calculation system. For HEO catalysts, it is necessary to build and optimize accurate thermodynamic and kinetic models. Comprehensive computational methods are the theoretical basis to predict and identify active sites for different chemical catalysis reactions over the HEO catalysts. To further enable computational screening and identification of catalysts with novel structures that are as active as or even higher than existing HEOs, machine learning would be a valuable tool once the training sample dataset is large enough.¹⁴¹
4. Diversified application and development. To fully use HEO's potential properties, it can be extended to photocatalysis, photothermal catalysis, biomass

conversion and solar cells, and more. The greatest challenge for the further development of promising new catalysts is scaling up to pilot-scale and industrial-scale use. Meanwhile, it is widely known that actual industrial production processes usually involve various reactions. Therefore, an efficient approach is necessary to design a reaction device filled with catalysts in series to accelerate each reaction for the achievement of multi-step coupled reactions. This is because almost every kind of element can be introduced into the structure of HEOs with unique catalytic activity to build a multifunctional catalyst. Therefore, HEOs can be efficiently designed for multi-step coupling reactions.

Overall, developing functionalized HEO catalysts for classical chemical catalytic reactions and designing novel HEO catalysts for targeted catalytic reactions are exciting directions. To this end, it is highly necessary to make continued efforts in the controllable preparation, in-depth structure analysis, and elaborate understanding of the physicochemical properties of HEOs. We believe that the enhanced performance of different catalytic reactions over HEOs could be achieved in both academia and industrial fields by improving HEOs and their derived catalysts in the near future.

ACKNOWLEDGMENTS

This work was financially supported by the National Natural Science Foundation of China (grant nos. 22125903 and 51872283), the Dalian Innovation Support Plan for High Level Talents (2019RT09), the Dalian National Laboratory for Clean Energy, CAS, DNL Cooperation Fund, CAS (DNL201912, DNL201915, DNL202016, and DNL202019), DICP (DICP ZZBS201802 and DICP I2020032), the Joint Fund of the Yulin University and the Dalian National Laboratory for Clean Energy (YLU-DNL Fund 2021002, the YLU-DNL Fund 2021009), and the China Postdoctoral Science Foundation (2021M693125).

AUTHOR CONTRIBUTIONS

The manuscript was written through the contributions of all authors. All authors have given approval to the final version of the manuscript.

DECLARATION OF INTERESTS

The authors declare no competing interests.

REFERENCES

1. Barles, S. (2010). Society, energy and materials: the contribution of urban metabolism studies to sustainable urban development issues. *J. Environ. Plan. Manag.* 53, 439–455. <https://doi.org/10.1080/09640561003703772>.
2. Gutfleisch, O., Willard, M.A., Bruck, E., Chen, C.H., Sankar, S.G., and Liu, J.P. (2011). Magnetic materials and devices for the 21st century: stronger, lighter, and more energy efficient. *Adv. Mater.* 23, 821–842. <https://doi.org/10.1002/adma.201002180>.
3. Sun, L.G., Wu, G., Wang, Q., and Lu, J. (2020). Nanostructural metallic materials: structures and mechanical properties. *Mater. Today* 38, 114–135. <https://doi.org/10.1016/j.mattod.2020.04.005>.
4. Zykova, A.P., Tarasov, S.Y., Chumaevskiy, A.V., and Kolubaev, E.A. (2020). A review of friction stir processing of structural metallic materials: process, properties, and methods. *Metals* 10, 772. <https://doi.org/10.3390/met10060772>.
5. Ma, Y., Ma, Y., Wang, Q., Schweidler, S., Botros, M., Fu, T., Hahn, H., Brezesinski, T., and Breitung, B. (2021). High-entropy energy materials: challenges and new opportunities. *Energy Environ. Sci.* 14, 2883–2905. <https://doi.org/10.1039/d1ee00505g>.
6. Oses, C., Toher, C., and Curtarolo, S. (2020). High-entropy ceramics. *Nat. Rev. Mater.* 5, 295–309. <https://doi.org/10.1038/s41578-019-0170-8>.
7. Sun, Y.F., and Dai, S. (2021). High-entropy materials for catalysis: a new Frontier. *Sci. Adv.* 7, 1600. <https://doi.org/10.1126/sciadv.abg1600>.
8. Chen, J., Liu, W., Liu, J., Zhang, X., Yuan, M., Zhao, Y., Yan, J., Hou, M., Yan, J., Kunz, M., et al. (2019). Stability and compressibility of cation-doped high-entropy oxide MgCoNiCuZnO₅. *J. Phys. Chem. C* 123, 17735–17744. <https://doi.org/10.1021/acs.jpcc.9b04992>.
9. Amiri, A., and Shahbazian-Yassar, R. (2021). Recent progress of high-entropy materials for energy storage and conversion. *J. Mater. Chem. A* 9, 782–823. <https://doi.org/10.1039/d0ta09578h>.
10. Sarkar, A., Wang, Q., Schiele, A., Chellali, M.R., Bhattacharya, S.S., Wang, D., Brezesinski, T., Hahn, H., Velasco, L., and Breitung, B. (2019). High-entropy oxides: fundamental aspects and electrochemical properties (Adv. Mater. 26/2019). *Adv. Mater.* 31, e1806236. <https://doi.org/10.1002/adma.201970189>.
11. Zhan, C.H., Xu, Y., Bu, L.Z., Zhu, H.Z., Feng, Y.G., Yang, T., Zhang, Y., Yang, Z.Q., Huang, B.L., Shao, Q., and Huang, X.Q. (2021).

- Subnanometer high-entropy alloy nanowires enable remarkable hydrogen oxidation catalysis. *Nat. Commun.* **12**, 6261. <https://doi.org/10.1038/s41467-021-26425-2>.
- Du, Z., Wu, C., Chen, Y., Cao, Z., Hu, R., Zhang, Y., Gu, J., Cui, Y., Chen, H., Shi, Y., et al. (2021). High-entropy atomic layers of transition-metal carbides (MXenes). *Adv. Mater.* **33**, 2101473. <https://doi.org/10.1002/adma.202101473>.
 - Wang, T., Chen, H., Yang, Z., Liang, J., and Dai, S. (2020). High-entropy perovskite fluorides: a new platform for oxygen evolution catalysis. *J. Am. Chem. Soc.* **142**, 4550–4554. <https://doi.org/10.1021/jacs.9b12377>.
 - Cui, M., Yang, C., Li, B., Dong, Q., Wu, M., Hwang, S., Xie, H., Wang, X., Wang, G., and Hu, L. (2020). High-entropy metal sulfide nanoparticles promise high-performance oxygen evolution reaction. *Adv. Energy Mater.* **11**, 2002887. <https://doi.org/10.1002/aenm.202002887>.
 - Jin, Z., Lyu, J., Zhao, Y., Li, H., Chen, Z., Lin, X., Xie, G., Liu, X., Kai, J.J., Kai, J., Qiu, H.J., and Qiu, H. (2021). Top-down synthesis of noble metal particles on high-entropy oxide supports for electrocatalysis. *Chem. Mater.* **33**, 1771–1780. <https://doi.org/10.1021/acs.chemmater.0c04695>.
 - Rost, C.M., Sachet, E., Borman, T., Moballegh, A., Dickey, E.C., Hou, D., Jones, J.L., Curtarolo, S., and Maria, J.P. (2015). Entropy-stabilized oxides. *Nat. Commun.* **6**, 8485. <https://doi.org/10.1038/ncomms9485>.
 - Braun, J.L., Rost, C.M., Lim, M., Giri, A., Olson, D.H., Kotsolis, G.N., Stan, G., Brenner, D.W., Maria, J.P., and Hopkins, P.E. (2018). Charge-induced disorder controls the thermal conductivity of entropy-stabilized oxides. *Adv. Mater.* **30**, 1805004. <https://doi.org/10.1002/adma.201805004>.
 - Djenadic, R., Sarkar, A., Clemens, O., Loho, C., Botros, M., Chakravadhanula, V.S.K., Kübel, C., Bhattacharya, S.S., Gandhi, A.S., and Hahn, H. (2016). Multicomponent equiatomic rare earth oxides. *Mater. Res. Lett.* **5**, 102–109. <https://doi.org/10.1080/21663831.2016.1220433>.
 - Sharma, Y., Musico, B.L., Gao, X., Hua, C., May, A.F., Herklotz, A., Rastogi, A., Mandrus, D., Yan, J., Lee, H.N., et al. (2018). Single-crystal high entropy perovskite oxide epitaxial films. *Phys. Rev. Mater.* **2**, 060404. <https://doi.org/10.1103/physrevmaterials.2.060404>.
 - Dąbrowa, J., Stygar, M., Mikula, A., Knapik, A., Mroczka, K., Tejchman, W., Danielewski, M., and Martin, M. (2018). Synthesis and microstructure of the (Co,Cr,Fe,Mn,Ni)₃O₄ high entropy oxide characterized by spinel structure. *Mater. Lett.* **216**, 32–36. <https://doi.org/10.1016/j.matlet.2017.12.148>.
 - Hussain, I., Lamiel, C., Ahmad, M., Chen, Y., Shuang, S., Javed, M.S., Yang, Y., and Zhang, K. (2021). High entropy alloys as electrode material for supercapacitors: a review. *J. Energy Storage* **44**, 103405. <https://doi.org/10.1016/j.est.2021.103405>.
 - Luo, Y., Hao, S., Cai, S., Slade, T.J., Luo, Z.Z., Dravid, V.P., Wolverton, C., Yan, Q., and Kanatzidis, M.G. (2020). High thermoelectric performance in the new cubic semiconductor AgSnSbSe₃ by high-entropy engineering. *J. Am. Chem. Soc.* **142**, 15187–15198. <https://doi.org/10.1021/jacs.0c07803>.
 - Wang, B., Yao, Y., Yu, X., Wang, C., Wu, C., and Zou, Z. (2021). Understanding the enhanced catalytic activity of high entropy alloys: from theory to experiment. *J. Mater. Chem. A* **9**, 19410–19438. <https://doi.org/10.1039/d1ta02718b>.
 - Albedwawi, S.H., AlJaberi, A., Haidemenopoulos, G.N., and Polychronopoulou, K. (2021). High entropy oxides-exploring a paradigm of promising catalysts: a review. *Mater. Des.* **202**, 109534. <https://doi.org/10.1016/j.matdes.2021.109534>.
 - Wang, G., Qin, J., Feng, Y., Feng, B., Yang, S., Wang, Z., Zhao, Y., and Wei, J. (2020). Sol-gel synthesis of spherical mesoporous high-entropy oxides. *ACS Appl. Mater. Interfaces* **12**, 45155–45164. <https://doi.org/10.1021/acscami.0c11899>.
 - Shu, Y., Bao, J., Yang, S., Duan, X., and Zhang, P. (2020). Entropy-stabilized metal-CeO_x solid solutions for catalytic combustion of volatile organic compounds. *AIChE J.* **67**, 17046. <https://doi.org/10.1002/aic.17046>.
 - Xu, H., Zhang, Z., Liu, J., Do-Thanh, C.L., Chen, H., Xu, S., Lin, Q., Jiao, Y., Wang, J., Wang, Y., et al. (2020). Entropy-stabilized single-atom Pd catalysts via high-entropy fluorite oxide supports. *Nat. Commun.* **11**, 3908. <https://doi.org/10.1038/s41467-020-17738-9>.
 - Hou, S., Ma, X., Shu, Y., Bao, J., Zhang, Q., Chen, M., Zhang, P., and Dai, S. (2021). Self-regeneration of supported transition metals by a high entropy-driven principle. *Nat. Commun.* **12**, 5917. <https://doi.org/10.1038/s41467-021-26160-8>.
 - Chen, H., Lin, W., Zhang, Z., Jie, K., Mullins, D.R., Sang, X., Yang, S.-Z., Jafta, C.J., Bridges, C.A., Hu, X., et al. (2019). Mechanochemical synthesis of high entropy oxide materials under ambient conditions: dispersion of catalysts via entropy maximization. *ACS Mater. Lett.* **1**, 83–88. <https://doi.org/10.1021/acsmaterialslett.9b00064>.
 - Fracchia, M., Ghigna, P., Pozzi, T., Anselmi Tamburini, U., Colombo, V., Braglia, L., and Torelli, P. (2020). Stabilization by configurational entropy of the Cu(II) active site during CO oxidation on Mg_{0.2}Co_{0.2}Ni_{0.2}Cu_{0.2}Zn_{0.2}O. *J. Phys. Chem. Lett.* **11**, 3589–3593. <https://doi.org/10.1021/acs.jpcclett.0c00602>.
 - Zhai, S., Rojas, J., Ahlborg, N., Lim, K., Toney, M.F., Jin, H., Chueh, W.C., and Majumdar, A. (2018). The use of poly-cation oxides to lower the temperature of two-step thermochemical water splitting. *Energy Environ. Sci.* **11**, 2172–2178. <https://doi.org/10.1039/c8ee00050f>.
 - Feng, D., Dong, Y., Zhang, L., Ge, X., Zhang, W., Dai, S., and Qiao, Z.A. (2020). Holey lamellar high-entropy oxide as an ultra-high-activity heterogeneous catalyst for solvent-free aerobic oxidation of benzyl alcohol. *Angew. Chem. Int. Ed. Engl.* **132**, 19503–19509. <https://doi.org/10.1002/ange.202004892>.
 - Jin, Z., Lyu, J., Zhao, Y., Li, H., Lin, X., Xie, G., Liu, X., Kai, J.J., Kai, J., Qiu, H.J., and Qiu, H. (2020). Rugged high-entropy alloy nanowires with in-situ formed surface spinel oxide as highly stable electrocatalyst in Zn-Air batteries. *ACS Mater. Lett.* **2**, 1698–1706. <https://doi.org/10.1021/acsmaterialslett.0c00434>.
 - He, S., Somayaji, V., Wang, M., Lee, S.-H., Geng, Z., Zhu, S., Novello, P., Varanasi, C.V., and Liu, J. (2021). High entropy spinel oxide for efficient electrochemical oxidation of ammonia. *Nano Res.* **1**. <https://doi.org/10.1007/s12274-021-3665-8>.
 - Zheng, Y., Yi, Y., Fan, M., Liu, H., Li, X., Zhang, R., Li, M., and Qiao, Z.-A. (2019). A high-entropy metal oxide as chemical anchor of polysulfide for lithium-sulfur batteries. *Energy Storage Mater.* **23**, 678–683. <https://doi.org/10.1016/j.ensm.2019.02.030>.
 - Tang, L., Li, Z., Chen, K., Li, C., Zhang, X., and An, L. (2021). High-entropy oxides based on valence combinations: design and practice. *J. Am. Ceram. Soc.* **104**, 1953–1958. <https://doi.org/10.1111/jace.17659>.
 - Hong, W., Chen, F., Shen, Q., Han, Y.H., Fahrenholtz, W.G., and Zhang, L. (2019). Microstructural evolution and mechanical properties of (Mg,Co,Ni,Cu,Zn)O high-entropy ceramics. *J. Am. Ceram. Soc.* **102**, 2228–2237. <https://doi.org/10.1111/jace.16075>.
 - Gild, J., Samiee, M., Braun, J.L., Harrington, T., Vega, H., Hopkins, P.E., Vecchio, K., and Luo, J. (2018). High-entropy fluorite oxides. *J. Eur. Ceram. Soc.* **38**, 3578–3584. <https://doi.org/10.1016/j.jeurceramsoc.2018.04.010>.
 - Chen, K., Pei, X., Tang, L., Cheng, H., Li, Z., Li, C., Zhang, X., and An, L. (2018). A five-component entropy-stabilized fluorite oxide. *J. Eur. Ceram. Soc.* **38**, 4161–4164. <https://doi.org/10.1016/j.jeurceramsoc.2018.04.063>.
 - Zhivulin, V.E., Trofimov, E.A., Gudkova, S.A., Pashkev, I.V., Punda, A.Y., Gavrilak, M., Zaitseva, O.V., Taskaev, S.V., Podgornov, F.V., Darwish, M.A., et al. (2021). Polysubstituted high-entropy LaNd (Cr_{0.2}Mn_{0.2}Fe_{0.2}Co_{0.2}Ni_{0.2}) O₃ perovskites: correlation of the electrical and magnetic properties. *Nanomaterials* **11**, 1014. <https://doi.org/10.3390/nano11041014>.
 - Bérardan, D., Franger, S., Meena, A.K., and Drago, N. (2016). Room temperature lithium superionic conductivity in high entropy oxides. *J. Mater. Chem. A* **4**, 9536–9541. <https://doi.org/10.1039/c6ta03249d>.
 - Chen, H., Sun, Y., Yang, S., Wang, H., Dmowski, W., Egami, T., and Dai, S. (2020). Self-regenerative noble metal catalysts supported on high-entropy oxides. *Chem. Commun.* **56**, 15056–15059. <https://doi.org/10.1039/d0cc05860b>.
 - Sarkar, A., Loho, C., Velasco, L., Thomas, T., Bhattacharya, S.S., Hahn, H., and Djenadic, R. (2017). Multicomponent equiatomic rare earth oxides with a narrow band gap and associated praseodymium multivalency. *Dalton Trans.* **46**, 12167–12176. <https://doi.org/10.1039/c7dt02077e>.
 - Usharani, N.J., Bhandarkar, A., Subramanian, S., and Bhattacharya, S.S. (2020). Antiferromagnetism in a nanocrystalline high

- entropy oxide (Co,Cu,Mg,Ni,Zn)O: magnetic constituents and surface anisotropy leading to lattice distortion. *Acta Mater.* 200, 526–536. <https://doi.org/10.1016/j.actamat.2020.09.034>.
45. Sarkar, A., Velasco, L., Wang, D., Wang, Q., Talasila, G., de Biasi, L., Kubel, C., Brezesinski, T., Bhattacharya, S.S., Hahn, H., and Breitung, B. (2018). High entropy oxides for reversible energy storage. *Nat. Commun.* 9, 3400. <https://doi.org/10.1038/s41467-018-05774-5>.
 46. Sarkar, A., Djenadic, R., Wang, D., Hein, C., Kautenburger, R., Clemens, O., and Hahn, H. (2018). Rare earth and transition metal based entropy stabilised perovskite type oxides. *J. Eur. Ceram. Soc.* 38, 2318–2327. <https://doi.org/10.1016/j.jeurceramsoc.2017.12.058>.
 47. Witte, R., Sarkar, A., Kruk, R., Eggert, B., Brand, R.A., Wende, H., and Hahn, H. (2019). High-entropy oxides: an emerging prospect for magnetic rare-earth transition metal perovskites. *Phys. Rev. Mater.* 3, 034406. <https://doi.org/10.1103/physrevmaterials.3.034406>.
 48. Sarkar, A., Djenadic, R., Usharani, N.J., Sanghvi, K.P., Chakravadhanula, V.S.K., Gandhi, A.S., Hahn, H., and Bhattacharya, S.S. (2017). Nanocrystalline multicomponent entropy stabilised transition metal oxides. *J. Eur. Ceram. Soc.* 37, 747–754. <https://doi.org/10.1016/j.jeurceramsoc.2016.09.018>.
 49. Gautam, A., and Ahmad, M.I. (2021). Low-temperature synthesis of five component single phase high entropy oxide. *Ceram. Int.* 47, 22225–22228. <https://doi.org/10.1016/j.ceramint.2021.04.128>.
 50. Sushil, J., Kumar, A., Gautam, A., and Ahmad, M.I. (2021). High entropy phase evolution and fine structure of five component oxide (Mg, Co, Ni, Cu, Zn)O by citrate gel method. *Mater. Chem. Phys.* 259, 124014. <https://doi.org/10.1016/j.matchemphys.2020.124014>.
 51. Saghir, A.V., Beidokhti, S.M., Khaki, J.V., and Salimi, A. (2021). One-step synthesis of single-phase (Co, Mg, Ni, Cu, Zn) O High entropy oxide nanoparticles through SCS procedure: thermodynamics and experimental evaluation. *J. Eur. Ceram. Soc.* 41, 563–579. <https://doi.org/10.1016/j.jeurceramsoc.2020.08.044>.
 52. Mao, A., Xiang, H., Zhang, Z.G., Zhang, Z., Kuramoto, K., Yu, H., and Ran, S. (2019). Solution combustion synthesis and magnetic property of rock-salt (Co_{0.2}Cu_{0.2}Mg_{0.2}Ni_{0.2}Zn_{0.2})O high-entropy oxide nanocrystalline powder. *J. Magn. Mater.* 484, 245–252. <https://doi.org/10.1016/j.jmmm.2019.04.023>.
 53. Aali, H., Mollazadeh, S., and Khaki, J.V. (2018). Single-phase magnetite with high saturation magnetization synthesized via modified solution combustion synthesis procedure. *Ceram. Int.* 44, 20267–20274. <https://doi.org/10.1016/j.ceramint.2018.08.012>.
 54. Park, T., Javadinejad, H.R., Kim, Y.-K., Chang, H.J., Choi, H., Woong, C., Ashong, A.N., Lee, Y.S., and Kim, J.H. (2022). Effect of processing route on the crystal structure and physical properties of bixbyite high-entropy oxides. *J. Alloys Compd.* 893, 162108. <https://doi.org/10.1016/j.jallcom.2021.162108>.
 55. Dąbrowa, J., Olszewska, A., Falkenstein, A., Schwab, C., Szymczak, M., Zajusz, M., Możdzierz, M., Mikuła, A., Zielińska, K., Berent, K., et al. (2020). An innovative approach to design SOFC air electrode materials: high entropy La_{1-x}Sr_x(Co,Cr,Fe,Mn,Ni)O_{3-δ} (x=0,0.1,0.2,0.3) perovskites synthesized by the sol-gel method. *J. Mater. Chem. A* 8, 24455–24468. <https://doi.org/10.1039/d0ta06356h>.
 56. Riley, C., De La Riva, A., Park, J.E., Percival, S.J., Benavidez, A., Coker, E.N., Aidun, R.E., Paisley, E.A., Datye, A., and Chou, S.S. (2021). A high entropy oxide designed to catalyze CO oxidation without precious metals. *ACS Appl. Mater. Interfaces* 13, 8120–8128. <https://doi.org/10.1021/acsami.0c17446>.
 57. Okejiri, F., Zhang, Z., Liu, J., Liu, M., Yang, S., and Dai, S. (2020). Room-temperature synthesis of high-entropy perovskite oxide nanoparticle catalysts through ultrasonication-based method. *ChemSusChem* 13, 111–115. <https://doi.org/10.1002/cssc.201902705>.
 58. Spiridigliozzi, L., Ferone, C., Cioffi, R., Accardo, G., Frattini, D., and Dell'Agli, G. (2020). Entropy-stabilized oxides owning fluorite structure obtained by hydrothermal treatment. *Materials* 13, 558. <https://doi.org/10.3390/ma13030558>.
 59. Shaw, S.K., Gangwar, A., Sharma, A., Alla, S.K., Kavita, S., Vasundhara, M., Meena, S.S., Maiti, P., and Prasad, N.K. (2021). Structural and magnetic properties of nanocrystalline equi-atomic spinel high-entropy oxide (AlCoFeMnNi)₃O₄ synthesised by microwave assisted co-precipitation technique. *J. Alloys Compd.* 878, 160269. <https://doi.org/10.1016/j.jallcom.2021.160269>.
 60. Park, T.S., Adomako, N.K., Ashong, A.N., Kim, Y.K., Yang, S.M., and Kim, J.H. (2021). Interfacial structure and physical properties of high-entropy oxide coatings prepared via atmospheric plasma spraying. *Coatings* 11, 755. <https://doi.org/10.3390/coatings11070755>.
 61. Mao, H.R., Guo, R.F., Cao, Y., Jin, S.B., Qiu, X.M., and Shen, P. (2021). Ultrafast densification of high-entropy oxide (La_{0.2}Nd_{0.2}Sm_{0.2}Eu_{0.2}Gd_{0.2})₂Zr₂O₇ by reactive flash sintering. *J. Eur. Ceram. Soc.* 41, 2855–2860. <https://doi.org/10.1016/j.jeurceramsoc.2020.11.052>.
 62. Zhao, W., Yang, F., Liu, Z., Chen, H., Shao, Z., Zhang, X., Wang, K., and Xue, L. (2021). A novel (La_{0.2}Sm_{0.2}Eu_{0.2}Gd_{0.2}Tm_{0.2})₂Zr₂O₇ high-entropy ceramic nanofiber with excellent thermal stability. *Ceram. Int.* 47, 29379–29385. <https://doi.org/10.1016/j.ceramint.2021.07.105>.
 63. Al Soubaihi, R., Saoud, K., and Dutta, J. (2018). Critical review of low-temperature CO oxidation and hysteresis phenomenon on heterogeneous catalysts. *Catalysts* 8, 660. <https://doi.org/10.3390/catal8120660>.
 64. Liu, Q., Mi, J., Chen, X., Wang, S., Chen, J., and Li, J. (2021). Effects of phosphorus modification on the catalytic properties and performance of CuCeZr mixed metal catalyst for simultaneous removal of CO and NO_x. *Chem. Eng. J.* 423, 130228. <https://doi.org/10.1016/j.cej.2021.130228>.
 65. DeSario, P.A., Pitman, C.L., Delia, D.J., Driscoll, D.M., Maynes, A.J., Morris, J.R., Pennington, A.M., Brintlinger, T.H., Rolison, D.R., and Pietron, J.J. (2019). Low-temperature CO oxidation at persistent low-valent Cu nanoparticles on TiO₂ aerogels. *Appl. Catal. B Environ.* 252, 205–213. <https://doi.org/10.1016/j.apcatb.2019.03.073>.
 66. van Spronsen, M.A., Frenken, J.W.M., and Groot, I.M.N. (2017). Surface science under reaction conditions: CO oxidation on Pt and Pd model catalysts. *Chem. Soc. Rev.* 46, 4347–4374. <https://doi.org/10.1039/c7cs00045f>.
 67. Kim, H.Y., Lee, H.M., and Henkelman, G. (2012). CO oxidation mechanism on CeO₂-supported Au nanoparticles. *J. Am. Chem. Soc.* 134, 1560–1570. <https://doi.org/10.1021/ja207510v>.
 68. Tavani, F., Fracchia, M., Tofoni, A., Braglia, L., Jouve, A., Morandi, S., Manzoli, M., Torelli, P., Ghigna, P., and D'Angelo, P. (2021). Structural and mechanistic insights into low-temperature CO oxidation over a prototypical high entropy oxide by Cu L-edge operando soft X-ray absorption spectroscopy. *Phys. Chem. Chem. Phys.* 23, 26575–26584. <https://doi.org/10.1039/d1cp03946f>.
 69. Zhang, Z., Yang, S., Hu, X., Xu, H., Peng, H., Liu, M., Thapaliya, B.P., Jie, K., Zhao, J., Liu, J., et al. (2019). Mechanochemical nonhydrolytic sol-gel-strategy for the production of mesoporous multimetallic oxides. *Chem. Mater.* 31, 5529–5536. <https://doi.org/10.1021/acs.chemmater.9b01244>.
 70. Chen, H., Jie, K., Jafta, C.J., Yang, Z., Yao, S., Liu, M., Zhang, Z., Liu, J., Chi, M., Fu, J., and Dai, S. (2020). An ultra-stable heterostructured oxide catalyst based on high-entropy materials: a new strategy toward catalyst stabilization via synergistic interfacial interaction. *Appl. Catal. B Environ.* 276, 119155. <https://doi.org/10.1016/j.apcatb.2020.119155>.
 71. Chen, H., Fu, J., Zhang, P., Peng, H., Abney, C.W., Jie, K., Liu, X., Chi, M., and Dai, S. (2018). Entropy-stabilized metal oxide solid solutions as CO oxidation catalysts with high-temperature stability. *J. Mater. Chem. A* 6, 11129–11133. <https://doi.org/10.1039/c8ta01772g>.
 72. Zhao, J., Bao, J., Yang, S., Niu, Q., Xie, R., Zhang, Q., Chen, M., Zhang, P., and Dai, S. (2021). Exsolution-dissolution of supported metals on high-entropy Co₃MnNiCuZnOx: toward sintering-resistant catalysis. *ACS Catal.* 11, 12247–12257. <https://doi.org/10.1021/acscatal.1c03228>.
 73. Mori, K., Hashimoto, N., Kamiuchi, N., Yoshida, H., Kobayashi, H., and Yamashita, H. (2021). Hydrogen spillover-driven synthesis of high-entropy alloy nanoparticles as a robust catalyst for CO₂ hydrogenation. *Nat. Commun.* 12, 3884. <https://doi.org/10.1038/s41467-021-24228-z>.
 74. Pedersen, J.K., Batchelor, T.A.A., Bagger, A., and Rossmel, J. (2020). High-entropy alloys as catalysts for the CO₂ and CO reduction reactions. *ACS Catal.* 10, 2169–2176. <https://doi.org/10.1021/acscatal.9b04343>.
 75. Deng, C., Wu, P., Zhu, L., He, J., Tao, D., Lu, L., He, M., Hua, M., Li, H., and Zhu, W. (2020).

- High-entropy oxide stabilized molybdenum oxide via high temperature for deep oxidative desulfurization. *Appl. Mater. Today* 20, 100680. <https://doi.org/10.1016/j.apmt.2020.100680>.
76. Li, T., Yao, Y., Huang, Z., Xie, P., Liu, Z., Yang, M., Gao, J., Zeng, K., Brozyna, A.H., Pastel, G., et al. (2021). Denary oxide nanoparticles as highly stable catalysts for methane combustion. *Nat. Catal.* 4, 62–70. <https://doi.org/10.1038/s41929-020-00554-1>.
77. Tatar, D., Kojcinovic, J., Markovic, B., Szechenyi, A., Miletic, A., Nagy, S.B., Ziegenheim, S., Szenti, I., Sapi, A., Kukovec, A., et al. (2021). Sol-gel synthesis of ceria-zirconia-based high-entropy oxides as high-promotion catalysts for the synthesis of 1,2-diketones from aldehyde. *Molecules* 26, 6115. <https://doi.org/10.3390/molecules26206115>.
78. Liu, H., Xia, J., Zhang, N., Cheng, H., Bi, W., Zu, X., Chu, W., Wu, H., Wu, C., and Xie, Y. (2021). Solid-liquid phase transition induced electrocatalytic switching from hydrogen evolution to highly selective CO₂ reduction. *Nat. Catal.* 4, 202–211. <https://doi.org/10.1038/s41929-021-00576-3>.
79. Li, F., Medvedeva, X.V., Medvedev, J.J., Khairullina, E., Engelhardt, H., Chandrasekar, S., Guo, Y., Jin, J., Lee, A., Thérien-Aubin, H., et al. (2021). Interplay of electrochemical and electrical effects induces structural transformations in electrocatalysts. *Nat. Catal.* 4, 479–487. <https://doi.org/10.1038/s41929-021-00624-y>.
80. Zhai, P., Xia, M., Wu, Y., Zhang, G., Gao, J., Zhang, B., Cao, S., Zhang, Y., Li, Z., Fan, Z., et al. (2021). Engineering single-atomic ruthenium catalytic sites on defective nickel-iron layered double hydroxide for overall water splitting. *Nat. Commun.* 12, 4587. <https://doi.org/10.1038/s41467-021-24828-9>.
81. Li, Z., Wang, Q., Bai, X., Wang, M., Yang, Z., Du, Y., Sterbinsky, G.E., Wu, D., Yang, Z., Tian, H., et al. (2021). Doping-modulated strain control of bifunctional electrocatalysis for rechargeable zinc-air batteries. *Energy Environ. Sci.* 14, 5035–5043. <https://doi.org/10.1039/d1ee01271a>.
82. Gong, F., Liu, M., Ye, S., Gong, L., Zeng, G., Xu, L., Zhang, X., Zhang, Y., Zhou, L., Fang, S., and Liu, J. (2021). All-pH stable sandwich-structured MoO₃/MoS₂/C hollow nanoreactors for enhanced electrochemical hydrogen evolution. *Adv. Funct. Mater.* 31, 2101715. <https://doi.org/10.1002/adfm.202101715>.
83. Jiang, X., Jang, H., Liu, S., Li, Z., Kim, M.G., Li, C., Qin, Q., Liu, X., and Cho, J. (2021). The heterostructure of Ru₂P/WO₃/NPC synergistically promotes H₂O dissociation for improved hydrogen evolution. *Angew. Chem. Int. Ed. Engl.* 133, 4156–4162. <https://doi.org/10.1002/ange.202014411>.
84. Zhao, Y., Li, F., Li, W., Li, Y., Liu, C., Zhao, Z., Shan, Y., Ji, Y., and Sun, L. (2021). Identification of M-NH₂-NH₂ intermediate and rate determining step for nitrogen reduction with bioinspired sulfur-bonded FeW catalyst. *Angew. Chem. Int. Ed. Engl.* 133, 20494–20504. <https://doi.org/10.1002/ange.202104918>.
85. Lin, G., Ju, Q., Guo, X., Zhao, W., Adimi, S., Ye, J., Bi, Q., Wang, J., Yang, M., and Huang, F. (2021). Intrinsic electron localization of metastable MoS₂ boosts electrocatalytic nitrogen reduction to ammonia. *Adv. Mater.* 33, 2007509. <https://doi.org/10.1002/adma.202007509>.
86. Yang, D., Ni, B., and Wang, X. (2020). Heterogeneous catalysts with well-defined active metal sites toward CO₂ electrocatalytic reduction. *Adv. Energy Mater.* 10, 2001142. <https://doi.org/10.1002/aenm.202001142>.
87. Zhang, Y., Dong, L.Z., Li, S., Huang, X., Chang, J.N., Wang, J.H., Zhou, J., Li, S.L., and Lan, Y.Q. (2021). Coordination environment dependent selectivity of single-site-Cu enriched crystalline porous catalysts in CO₂ reduction to CH₄. *Nat. Commun.* 12, 6390. <https://doi.org/10.1038/s41467-021-26724-8>.
88. Liu, W.J., Xu, Z., Zhao, D., Pan, X.Q., Li, H.C., Hu, X., Fan, Z.Y., Wang, W.K., Zhao, G.H., Jin, S., et al. (2020). Efficient electrochemical production of glucaric acid and H₂ via glucose electrolysis. *Nat. Commun.* 11, 265. <https://doi.org/10.1038/s41467-019-14157-3>.
89. Geng, S.K., Zheng, Y., Li, S.Q., Su, H., Zhao, X., Hu, J., Shu, H.B., Jaroniec, M., Chen, P., Liu, Q.H., and Qiao, S.Z. (2021). Nickel ferrocyanide as a high-performance urea oxidation electrocatalyst. *Nat. Energy* 6, 904–912. <https://doi.org/10.1038/s41560-021-00899-2>.
90. Yin, K., Chao, Y., Lv, F., Tao, L., Zhang, W., Lu, S., Li, M., Zhang, Q., Gu, L., Li, H., and Guo, S. (2021). One nanometer PtIr nanowires as high-efficiency bifunctional catalysts for electrosynthesis of ethanol into high value-added multicarbon compound coupled with hydrogen production. *J. Am. Chem. Soc.* 143, 10822–10827. <https://doi.org/10.1021/jacs.1c04626>.
91. Li, T., Li, S., Liu, Q., Yin, J., Sun, D., Zhang, M., Xu, L., Tang, Y., and Zhang, Y. (2020). Immobilization of Ni₃Co nanoparticles into N-doped carbon nanotube/nanofiber integrated hierarchically branched architectures toward efficient overall water splitting. *Adv. Sci.* 7, 1902371. <https://doi.org/10.1002/advs.201902371>.
92. Fu, G., Wang, J., Chen, Y., Liu, Y., Tang, Y., Goodenough, J.B., and Lee, J.-M. (2018). Exploring indium-based ternary thiospinel as conceivable high-potential air-cathode for rechargeable Zn-Air batteries. *Adv. Energy Mater.* 8, 1802263. <https://doi.org/10.1002/aenm.201802263>.
93. Fu, M., Ma, X., Zhao, K., Li, X., and Su, D. (2021). High-entropy materials for energy-related applications. *iScience* 24, 102177. <https://doi.org/10.1016/j.isci.2021.102177>.
94. Wang, D., Liu, Z., Du, S., Zhang, Y., Li, H., Xiao, Z., Chen, W., Chen, R., Wang, Y., Zou, Y., and Wang, S. (2019). Low-temperature synthesis of small-sized high-entropy oxides for water oxidation. *J. Mater. Chem. A* 7, 24211–24216. <https://doi.org/10.1039/c9ta08740k>.
95. Gu, K., Wang, D., Xie, C., Wang, T., Huang, G., Liu, Y., Zou, Y., Tao, L., and Wang, S. (2021). Defect-rich high-entropy oxide nanosheets for efficient 5-hydroxymethylfurfural electro-oxidation. *Angew. Chem. Int. Ed. Engl.* 133, 20415–20420. <https://doi.org/10.1002/ange.202107390>.
96. Yao, Y., Hu, S., Chen, W., Huang, Z.-Q., Wei, W., Yao, T., Liu, R., Zang, K., Wang, X., Wu, G., et al. (2019). Engineering the electronic structure of single atom Ru sites via compressive strain boosts acidic water oxidation electrocatalysis. *Nat. Catal.* 2, 304–313. <https://doi.org/10.1038/s41929-019-0246-2>.
97. Li, Y., Wang, Y., Lu, J., Yang, B., San, X., and Wu, Z.-S. (2020). 2D intrinsically defective RuO₂/Graphene heterostructures as All-pH efficient oxygen evolving electrocatalysts with unprecedented activity. *Nano Energy* 78, 105185. <https://doi.org/10.1016/j.nanoen.2020.105185>.
98. Gao, J.J., Tao, H.B., and Liu, B. (2021). Progress of nonprecious-metal-based electrocatalysts for oxygen evolution in acidic media. *Adv. Mater.* 33, 2003786. <https://doi.org/10.1002/adma.202003786>.
99. Shan, J., Ling, T., Davey, K., Zheng, Y., and Qiao, S.Z. (2019). Transition-metal-doped RuIr bifunctional nanocrystals for overall water splitting in acidic environments. *Adv. Mater.* 31, 1900510. <https://doi.org/10.1002/adma.201900510>.
100. Rao, R.R., Kolb, M.J., Giordano, L., Pedersen, A.F., Katayama, Y., Hwang, J., Mehta, A., You, H., Lunger, J.R., Zhou, H., et al. (2020). Operando identification of site-dependent water oxidation activity on ruthenium dioxide single-crystal surfaces. *Nat. Catal.* 3, 516–525. <https://doi.org/10.1038/s41929-020-0457-6>.
101. Chen, F.-Y., Wu, Z.-Y., Adler, Z., and Wang, H. (2021). Stability challenges of electrocatalytic oxygen evolution reaction: from mechanistic understanding to reactor design. *Joule* 5, 1704–1731. <https://doi.org/10.1016/j.joule.2021.05.005>.
102. Jiang, C., Yang, J., Han, X., Qi, H., Su, M., Zhao, D., Kang, L., Liu, X., Ye, J., Li, J., et al. (2021). Crystallinity-modulated Co_{2-x}V_xO₄ nanoplates for efficient electrochemical water oxidation. *ACS Catal.* 11, 14884–14891. <https://doi.org/10.1021/acscatal.1c04618>.
103. Zhang, J., Zhang, Q., and Feng, X.L. (2019). Support and interface effects in water-splitting electrocatalysts. *Adv. Mater.* 31, 1808167. <https://doi.org/10.1002/adma.201808167>.
104. Chen, J., Li, H., Fan, C., Meng, Q., Tang, Y., Qiu, X., Fu, G., and Ma, T. (2020). Dual single-atomic Ni-N₄ and Fe-N₄ sites constructing Janus hollow graphene for selective oxygen electrocatalysis. *Adv. Mater.* 32, 2003134. <https://doi.org/10.1002/adma.202003134>.
105. Song, L.N., Zhang, W., Wang, Y., Ge, X., Zou, L.C., Wang, H.F., Wang, X.X., Liu, Q.C., Li, F., and Xu, J.J. (2020). Tuning lithium-peroxide formation and decomposition routes with single-atom catalysts for lithium-oxygen batteries. *Nat. Commun.* 11, 2191. <https://doi.org/10.1038/s41467-020-15712-z>.
106. Sun, Y., Li, R., Chen, X., Wu, J., Xie, Y., Wang, X., Ma, K., Wang, L., Zhang, Z., Liao, Q., et al. (2021). A-site management prompts the

- dynamic reconstructed active phase of perovskite oxide OER catalysts. *Adv. Energy Mater.* **11**, 2003755. <https://doi.org/10.1002/aenm.202003755>.
107. Chen, Y., Sun, Y., Wang, M., Wang, J., Li, H., Xi, S., Wei, C., Xi, P., Sterbinsky, G.E., Freeland, J.W., et al. (2021). Lattice site-dependent metal leaching in perovskites toward a honeycomb-like water oxidation catalyst. *Sci. Adv.* **7**, eabk1788. <https://doi.org/10.1126/sciadv.abk1788>.
 108. Nguyen, T.X., Liao, Y.C., Lin, C.C., Su, Y.H., and Ting, J.M. (2021). Advanced high entropy perovskite oxide electrocatalyst for oxygen evolution reaction. *Adv. Funct. Mater.* **31**, 2101632. <https://doi.org/10.1002/adfm.202101632>.
 109. Tang, L., Fan, T., Chen, Z., Tian, J., Guo, H., Peng, M., Zuo, F., Fu, X., Li, M., Bu, Y., et al. (2021). Binary-dopant promoted lattice oxygen participation in OER on cobaltate electrocatalyst. *Chem. Eng. J.* **417**, 129324. <https://doi.org/10.1016/j.cej.2021.129324>.
 110. Wang, T., Fan, J., Do-Thanh, C.L., Suo, X., Yang, Z., Chen, H., Yuan, Y., Lyu, H., Yang, S., and Dai, S. (2021). Perovskite oxide-halide solid solutions: a platform for electrocatalysts. *Angew. Chem. Int. Ed. Engl.* **133**, 10041–10046. <https://doi.org/10.1002/ange.202101120>.
 111. Yang, L., Zhang, X., Yu, L., Hou, J., Zhou, Z., and Lv, R. (2021). Atomic Fe-N₄/C in flexible carbon fiber membrane as binder-free air cathode for Zn-Air batteries with stable cycling over 1000 h. *Adv. Mater.* **34**, 2105410. <https://doi.org/10.1002/adma.202105410>.
 112. Hu, X., Luo, G., Zhao, Q., Wu, D., Yang, T., Wen, J., Wang, R., Xu, C., and Hu, N. (2020). Ru single atoms on N-doped carbon by spatial confinement and ionic substitution strategies for high-performance Li-O₂ batteries. *J. Am. Chem. Soc.* **142**, 16776–16786. <https://doi.org/10.1021/jacs.0c07317>.
 113. Zhu, X., Tan, X., Wu, K.H., Haw, S.C., Pao, C.W., Su, B.J., Jiang, J., Smith, S.C., Chen, J.M., Amal, R., and Lu, X. (2021). Intrinsic ORR activity enhancement of Pt atomic sites by engineering the d-band center via local coordination tuning. *Angew. Chem. Int. Ed. Engl.* **133**, 22082–22088. <https://doi.org/10.1002/ange.202107790>.
 114. Sheng, K., Yi, Q., Chen, A.L., Wang, Y., Yan, Y., Nie, H., and Zhou, X. (2021). CoNi nanoparticles supported on N-doped bifunctional hollow carbon composites as high-performance ORR/OER catalysts for rechargeable Zn-Air batteries. *ACS Appl. Mater. Interfaces* **13**, 45394–45405. <https://doi.org/10.1021/acsami.1c10671>.
 115. Hu, H., Wang, J., Cui, B., Zheng, X., Lin, J., Deng, Y., and Han, X. (2021). Atomically dispersed selenium sites on nitrogen-doped carbon for efficient electrocatalytic oxygen reduction. *Angew. Chem. Int. Ed. Engl.* **61**, 202114441. <https://doi.org/10.1002/ange.202114441>.
 116. Zhao, M., Liu, H., Zhang, H., Chen, W., Sun, H., Wang, Z., Zhang, B., Song, L., Yang, Y., Ma, C., et al. (2021). A pH-universal ORR catalyst with single-atom iron sites derived from a double-layer MOF for superior flexible quasi-solid-state rechargeable Zn-air batteries. *Energy Environ. Sci.* **14**, 6455–6463. <https://doi.org/10.1039/d1ee01602d>.
 117. Kong, F., Si, R., Chen, N., Wang, Q., Li, J., Yin, G., Gu, M., Wang, J., Liu, L.-M., and Sun, X. (2022). Origin of hetero-nuclear Au-Co dual atoms for efficient acidic oxygen reduction. *Appl. Catal. B Environ.* **301**, 120782. <https://doi.org/10.1016/j.apcatb.2021.120782>.
 118. Fang, G., Gao, J., Lv, J., Jia, H., Li, H., Liu, W., Xie, G., Chen, Z., Huang, Y., Yuan, Q., et al. (2020). Multi-component nanoporous alloy/(oxy)hydroxide for bifunctional oxygen electrocatalysis and rechargeable Zn-air batteries. *Appl. Catal. B Environ.* **268**, 118431. <https://doi.org/10.1016/j.apcatb.2019.118431>.
 119. Li, T., Yao, Y., Ko, B.H., Huang, Z., Dong, Q., Gao, J., Chen, W., Li, J., Li, S., Wang, X., et al. (2021). Carbon-supported high-entropy oxide nanoparticles as stable electrocatalysts for oxygen reduction reactions. *Adv. Funct. Mater.* **31**, 2101561. <https://doi.org/10.1002/adfm.202010561>.
 120. Zhang, Y., Lyu, J., Zhao, Y.L., Hu, K., Chen, Z., Lin, X., Xie, G., Liu, X., and Qiu, H.J. (2021). *In-situ* coupling of Ag nanoparticles with high-entropy oxides as highly stable bifunctional catalysts for wearable Zn-Ag/Zn-air hybrid batteries. *Nanoscale* **13**, 16164–16171. <https://doi.org/10.1039/d1nr03539h>.
 121. Zhang, Y., Zhu, W., Wang, Y., Chen, W., Fang, J., Xu, Z., Xue, Y., Liu, D., Sui, R., Lv, Q., et al. (2021). Defective Ni₃S₂ nanowires as highly active electrocatalysts for ethanol oxidative upgrading. *Nano Res.* **15**, 2987–2993. <https://doi.org/10.1007/s12274-021-3930-x>.
 122. Qiu, Y., Zhang, J., Jin, J., Sun, J., Tang, H., Chen, Q., Zhang, Z., Sun, W., Meng, G., Xu, Q., et al. (2021). Construction of Pd-Zn dual sites to enhance the performance for ethanol electro-oxidation reaction. *Nat. Commun.* **12**, 5273. <https://doi.org/10.1038/s41467-021-25600-9>.
 123. Zhang, Y., Zhou, B., Wei, Z., Zhou, W., Wang, D., Tian, J., Wang, T., Zhao, S., Liu, J., Tao, L., and Wang, S. (2021). Coupling glucose-assisted Cu(I)/Cu(II) redox with electrochemical hydrogen production. *Adv. Mater.* **33**, 2104791. <https://doi.org/10.1002/adma.202104791>.
 124. Zhang, J., Gong, W., Yin, H., Wang, D., Zhang, Y., Zhang, H., Wang, G., and Zhao, H. (2021). *In-situ* growth of ultrathin Ni(OH)₂ nanosheets as catalyst for electrocatalytic oxidation reactions. *ChemSusChem* **14**, 2935–2942. <https://doi.org/10.1002/cssc.202100811>.
 125. Lu, Y., Liu, T., Dong, C.L., Yang, C., Zhou, L., Huang, Y.C., Li, Y., Zhou, B., Zou, Y., and Wang, S. (2021). Tailoring competitive adsorption sites by oxygen-vacancy on cobalt oxides to enhance the electrooxidation of biomass. *Adv. Mater.* **34**, e2107185.
 126. Xie, Y., Zhou, Z., Yang, N., and Zhao, G. (2021). An overall reaction integrated with highly selective oxidation of 5-hydroxymethylfurfural and efficient hydrogen evolution. *Adv. Funct. Mater.* **31**, 2102886. <https://doi.org/10.1002/adfm.202102886>.
 127. Liu, Y., Zhang, J., Li, Y., Qian, Q., Li, Z., Zhu, Y., and Zhang, G. (2020). Manipulating dehydrogenation kinetics through dual-doping Co₃N electrode enables highly efficient hydrazine oxidation assisting self-powered H₂ production. *Nat. Commun.* **11**, 1853. <https://doi.org/10.1038/s41467-020-15563-8>.
 128. Li, M., Xie, Z., Zheng, X., Li, L., Li, J., Ding, W., and Wei, Z. (2021). Revealing the regulation mechanism of Ir-MoO₂ interfacial chemical bonding for improving hydrogen oxidation reaction. *ACS Catal.* **11**, 14932–14940. <https://doi.org/10.1021/acscatal.1c04440>.
 129. Liu, J., Liu, Z., Wang, H., Liu, B., Zhao, N., Zhong, C., and Hu, W. (2021). Designing nanoporous Coral-like Pt nanowires architecture for methanol and ammonia oxidation reactions. *Adv. Funct. Mater.* **2110702**. <https://doi.org/10.1002/adfm.202110702>.
 130. Boyjoo, Y., Shi, H., Tian, Q., Liu, S., Liang, J., Wu, Z.-S., Jaroniec, M., and Liu, J. (2021). Engineering nanoreactors for metal-chalcogen batteries. *Energy Environ. Sci.* **14**, 540–575. <https://doi.org/10.1039/d0ee03316b>.
 131. Wang, J., and Han, W.Q. (2021). A review of heteroatom doped materials for advanced lithium-sulfur batteries. *Adv. Funct. Mater.* **32**, 2107166. <https://doi.org/10.1002/adfm.202107166>.
 132. Shi, H., Ren, X., Lu, J., Dong, C., Liu, J., Yang, Q., Chen, J., and Wu, Z.S. (2020). Lithium-sulfur batteries: dual-functional atomic zinc decorated hollow carbon nanoreactors for kinetically accelerated polysulfides conversion and dendrite free lithium sulfur batteries (Adv. Energy Mater. 39/2020). *Adv. Energy Mater.* **10**, 2070162. <https://doi.org/10.1002/aenm.202070162>.
 133. Tsao, Y., Gong, H., Chen, S., Chen, G., Liu, Y., Gao, T.Z., Cui, Y., and Bao, Z. (2021). A nickel-decorated carbon flower/sulfur cathode for lean-electrolyte lithium-sulfur batteries. *Adv. Energy Mater.* **11**, 2101449. <https://doi.org/10.1002/aenm.202101449>.
 134. Peng, H.-J., Huang, J.-Q., Cheng, X.-B., and Zhang, Q. (2017). Lithium-sulfur batteries: review on high-loading and high-energy lithium-sulfur batteries (Adv. Energy Mater. 24/2017). *Adv. Energy Mater.* **7**, 1770141. <https://doi.org/10.1002/aenm.201770141>.
 135. Tian, D., Song, X., Qiu, Y., Sun, X., Jiang, B., Zhao, C., Zhang, Y., Xu, X., Fan, L., and Zhang, N. (2021). Basal-plane-activated molybdenum sulfide nanosheets with suitable orbital orientation as efficient electrocatalysts for lithium-sulfur batteries. *ACS Nano* **15**, 16515–16524. <https://doi.org/10.1021/acsnano.1c06067>.
 136. Gao, H., Ning, S., Lin, J., and Kang, X. (2021). Molecular perturbation of 2D organic modifiers on porous carbon interlayer: promoted redox kinetics of polysulfides in lithium-sulfur batteries. *Energy Storage Mater.* **40**, 312–319. <https://doi.org/10.1016/j.ensm.2021.05.027>.
 137. Liu, X., Huang, J.Q., Zhang, Q., and Mai, L. (2017). Nanostructured metal oxides and sulfides for lithium-sulfur batteries. *Adv.*

- Mater. 29, 1601759. <https://doi.org/10.1002/adma.201601759>.
138. Wang, S., Feng, S., Liang, J., Su, Q., Zhao, F., Song, H., Zheng, M., Sun, Q., Song, Z., Jia, X., et al. (2021). Insight into MoS₂-Mon heterostructure to accelerate polysulfide conversion toward high-energy-density lithium-sulfur batteries. *Adv. Energy Mater.* 11, 2003314. <https://doi.org/10.1002/aenm.202003314>.
139. Du, Y., Huang, R., Lin, X., Khan, S., Zheng, B., and Fu, R. (2020). Template-free preparation of hierarchical porous carbon nanosheets for lithium-sulfur battery. *Langmuir* 36, 14507–14513. <https://doi.org/10.1021/acs.langmuir.0c02167>.
140. Tian, L.Y., Zhang, Z., Liu, S., Li, G.R., and Gao, X.P. (2021). High-entropy spinel oxide nanofibers as catalytic sulfur hosts promise the high gravimetric and volumetric capacities for lithium-sulfur batteries. *Energy Environ. Mater.* <https://doi.org/10.1002/eem2.12215>.
141. Seh, Z.W., Kibsgaard, J., Dickens, C.F., Chorkendorff, I., Nørskov, J.K., and Jaramillo, T.F. (2017). Combining theory and experiment in electrocatalysis: insights into materials design. *Science* 355, eaad4998. <https://doi.org/10.1126/science.aad4998>.